

OPTIMISED METHYLENE-BLUE DETECTION AND
QUANTIFICATION UTILISING CONVENTIONAL RAMAN
SPECTROSCOPY

By

Mahdieh Dashtbani Moghari

A THESIS SUBMITTED TO MACQUARIE UNIVERSITY
FOR THE DEGREE OF MASTER OF RESEARCH
DEPARTMENT OF PHYSICS AND ASTRONOMY
JUNE 2016



Except where acknowledged in the customary manner, the material presented in this thesis is, to the best of my knowledge, original and has not been submitted in whole or part for a degree in any university.

Mahdieh Dashtbani Moghari

Acknowledgements

First and foremost, I would like to express my deep sense of gratitude to my supervisors, Dr. Alex Fuerbach and Prof. Ewa Goldys, who supported me throughout this project. None of this would have been possible if not for their efforts.

I am also thankful to the admirable staff in the department of physics and astronomy for their wonderful support.

I wish to acknowledge Macquarie University for awarding me the international Research Training Pathway (iRTP) scholarship, and providing me financial support to attend conferences.

I would like to thank my parents, and my family as a whole, for their love and support throughout this project and my life.

Last but not least, thanks to my lovely friends, specially Abbas and Zahra, for making me feel special and being there when I needed them.

List of Publications

- Mahdieh Dashtbani Moghari, Ewa Goldys, Alex Fuerbach, "*optimal experimental conditions for minimising the limit of detection of Methylene blue by normal Raman spectroscopy*". (Presented in 24th Australian Conference on Microscopy and Microanalysis (ACMM24) - Feb 2016)
This work was awarded an Australian Microscopy and Microanalysis society (AMMS) bursary covering registration fee and travel expenses to attend ACMM24 conference.
- Mahdieh Dashtbani Moghari, Ewa Goldys, Alex Fuerbach, "*Quantification of Methylene Blue using normal Raman spectroscopy under different experimental conditions*". (Presented in Biofocus Research Conference - Dec 2015)

Abstract

Raman spectroscopy is a powerful technique based on specific molecular vibrations producing a characteristic "fingerprint spectrum" used for sample analysis. So far, the use of Raman quantitative analysis has not kept pace with its use for qualitative analysis due to some challenges, yet it has a great potential to be developed for measuring the intended property within the sample. Moreover, bulky laboratory Raman spectrometers are very pricey, complex and are designed to be as versatile as possible.

The main aim of this work is thus to perform a preliminary study that will enable the future advanced quantitative analysis and design of a much simpler, yet field-transportable system, that will allow the detection and quantification of minuscule amounts of toxins found in the environment and specific pesticides on the different plants. For that purpose, an existing Raman spectrometer is used to investigate the optimum conditions for the detection and quantification of a specific model-molecule with a well-known Raman spectrum, Methylene Blue (MB). In a systematic study, the influence of instrumental and sample-related parameters on the ability to detect very low concentrations of MB are therefore investigated. In particular, optimum excitation wavelength and power, laser spot size, and sample phase and configuration are found. Moreover, suitable methods for the calculation and minimisation of the limit of detection and quantification (LOD and LOQ) are applied under various experimental conditions. Finally, analytical models are established and the error of prediction are calculated and discussed.

The presented results offer clear guidelines for the quantification study, design and development of a field-transportable Raman analysis system, which will be the subject of a future PhD work.

Contents

Acknowledgements	iv
List of Publications	v
Abstract	vi
List of Figures	ix
List of Tables	xiii
1 Introduction	1
1.1 Raman spectroscopy technique	1
1.2 Motivation of the research	2
1.3 Research framework and objectives	3
1.4 Thesis overview and contributions	4
2 Background	5
2.1 The Raman effect	5
2.2 Raman spectroscopy	7
2.3 Comparing Raman spectroscopy with infrared spectroscopy	7
2.4 Advantages of Raman spectroscopy	8
2.5 Challenges of Raman spectroscopy and some possible solutions	9
2.6 Qualitative vs. Quantitative Raman	11
2.6.1 Qualitative analysis by Raman spectroscopy	11
2.6.2 Quantitative analysis by Raman spectroscopy	12
2.7 LOD and LOQ	13

3	Instrumentation, experimental and analysis methods	14
3.1	Raman Spectrometer	14
3.2	Methylene Blue	16
3.3	Experimental procedure	18
3.3.1	Sample preparation	19
3.3.2	Setup preparation	21
3.3.3	Raman spectra processing	21
3.3.4	Data analysis	23
4	Results and discussion	26
4.1	Selection of suitable excitation wavelength, exposure time, and laser power .	27
4.2	Reference System	30
4.3	LOD of MB in solid-state form	31
4.4	LOD of MB in aqueous solutions	33
4.4.1	LOD of MB in droplet samples	34
4.4.2	Modifying sample parameter	39
4.4.3	LOD of MB in aqueous solutions in the Al structure	40
4.5	Establishing analytical models and calculation of the errors	44
4.6	Comparison of the results of the quantitative analysis of MB in different sam- ple configurations	49
5	Conclusions and future works	51
5.1	Summary and research outcomes	51
5.1.1	Future works	54
A	Appendix	56
	List of Acronyms/Abbreviations	65
	References	66

List of Figures

2.1	Molecular energy diagram showing Rayleigh and Raman (Stokes and anti-Stokes) scattering as well as fluorescence. ν_0 , ν_R and ν_k are the frequencies of the incident light, the Raman-scattered light and the molecular vibration (Raman shift), respectively.	6
3.1	Schematic of the Renishaw InVia Raman spectrometer.	15
3.2	(a) Chemical structure of MB, Raman spectrum of (b) MB aqueous solution and (c) solid MB powder (Excitation wavelength: 532 nm, Power at sample: 1.75 mW, Exposure time: 10s).	17
3.3	Block diagram of experimental procedure followed in this study.	19
3.4	Block diagram of the signal processing steps that were followed in this study.	21
4.1	Normal Raman spectra of 100% MB aqueous solution in droplet from before baseline correction. The excitation wavelength is (a) 785 nm and (b) 532 nm (Objective lens used: 50x, Power at sample: 1.75 mW, Exposure time: 10s).	27
4.2	(a) Colour change of 100% MB aqueous solution from dark blue to yellow as a result of photochemical damage, (b) Normal Raman spectra of 100% MB aqueous solution: (1) before photobleaching (Objective lens in use: 50x, Excitation wavelength: 532 nm, Power at sample: 1.75 mW, Exposure time: 10s) and (2) after photobleaching (Objective lens in use: 50x, Excitation wavelength: 532 nm, Power at sample: 7 mW, Exposure time: 10s).	28

4.3	The intensity of the silicon Raman peak at 520.5 cm^{-1} vs. the solid angle of the microscope objectives in use while the excitation wavelength is 532 nm and the power at the sample is fixed at 1.75 mW . The vertical error bars show the peak intensity variations over five measurements from different locations of the silicon wafer and data points show the average peak intensity taken over five such measurements.	31
4.4	Coffee-ring effect of a MB droplet dried on a (a) regular silicon and (b) negatively charged silicon surface.	32
4.5	Sampling area of the (a) 50x, (b) 20x, and (c) 5x objective. In (a) and (b), the Raman peak intensities obtained from the (1) and (2) areas are much higher than those of the (3), (4), and (5) areas, while the spectral differences are negligible in the (1) and (2) areas of (c).	32
4.6	The intensity of the MB Raman peak at 1625 cm^{-1} vs. MB concentration obtained using the 5x objective lens from MB solutions in droplet forms (Excitation wavelength: 532 nm , Power at sample: 1.75 mW , Exposure time: 10s).	34
4.7	The intensity of the MB Raman peak at 1625 cm^{-1} vs. MB concentration obtained using the 50x objective lens from MB solutions in droplet forms (Excitation wavelength: 532 nm , Power at sample: 1.75 mW , Exposure time: 10s).	35
4.8	The intensity of the MB Raman peak at 1625 cm^{-1} vs. MB concentration obtained using the 20x objective lens from MB solutions in droplet forms (Excitation wavelength: 532 nm , Power at sample: 1.75 mW , Exposure time: 10s).	35
4.9	Schematic drawing demonstrating the origin of out-of-focus contributions to Raman signals. Photons originating at A, B and C which traverse paths APD, BPF and CPE will pass through P and thus through the confocal aperture. Summing all the similar contributions throughout the extended illumination volume leads to a non-negligible out-of-focus signal [74].	36
4.10	(a) Aluminium structure designed as sample holder, (b) MB solution in the aluminium structure under the microscope of the Raman spectrometer. . . .	39
4.11	The intensity of the MB Raman peak at 1625 cm^{-1} vs. MB concentration obtained using the 5x objective lens from MB solutions in the aluminium structure (Excitation wavelength: 532 nm , Power at sample: 1.75 mW , Exposure time: 10s).	40

4.12	Intensity of the MB Raman peak at 1625 cm^{-1} vs. MB concentration obtained using the 50x objective lens from MB solutions in the aluminium structure (Excitation wavelength: 532 nm, Power at sample: 1.75 mW, Exposure time: 10s).	41
4.13	Intensity of the MB Raman peak at 1625 cm^{-1} vs. MB concentration obtained using the 20x objective lens from MB solutions in the aluminium structure (Excitation wavelength: 532 nm, Power at sample: 1.75 mW, Exposure time: 10s).	41
4.14	UV-Vis absorption spectrum of MB aqueous solution [78].	43
4.15	(a) The intensity of the MB Raman peak at 1625 cm^{-1} vs. MB concentration obtained using the 50x objective lens from MB droplets (Power at sample: 1.75 mW, Exposure time: 10s). *data marked with red circles is not used for constructing the calibration curve* (b) Residual values of the calibration curve obtained using the 50x objective lens from MB droplets.	46
4.16	(a) The intensity of the MB Raman peak at 1625 cm^{-1} vs. MB concentration obtained using the 20x objective lens from MB droplets (Power at sample: 1.75 mW, Exposure time: 10s). *data marked with red circles is not used for constructing the calibration curve* (b) Residual values of the calibration curve obtained using the 20x objective lens from MB droplets.	47
4.17	(a) The intensity of the MB Raman peak at 1625 cm^{-1} vs. MB concentration obtained using the 50x objective lens from MB solutions in the Al structure (Power at sample: 1.75 mW, Exposure time: 10s). *data marked with red circles is not used for constructing the calibration curve* (b) Residual values of the calibration curve obtained using the 50x objective lens from MB solutions in the Al structure.	48
4.18	(a) The intensity of the MB Raman peak at 1625 cm^{-1} vs. MB concentration obtained using the 20x objective lens from MB solutions in the Al structure (Power at sample: 1.75 mW, Exposure time: 10s). *data marked with red circles is not used for constructing the calibration curve*(b) Residual values of the calibration curve obtained using the 20x objective lens from MB solutions in the Al structure.	49
A.1	The photograph of our Renishaw InVia Raman spectrometer.	57
A.2	Raman spectrum of 25% MB aqueous solution (a) before and (b) after baseline correction.	57

A.3	Raman spectra of silicon wafer obtained using the 50x, 20x, and 5x objective lenses (Excitation wavelength: 532 nm, Power at sample: 1.75 mW, Exposure time: 10s).	58
A.4	The intensity of the MB Raman peak at 1625 cm^{-1} vs. MB concentration obtained using the 5x objective lens from MB droplets dried on the surface of negatively charged silicon (Excitation wavelength: 532 nm, Power at sample: 1.75 mW, Exposure time:10s).	58
A.5	Raman spectra of MB droplets in different concentrations after baseline correction (Only five spectra are plotted for better clarity). [Objective lens in use: 50x, Excitation wavelength: 532 nm, Power at sample: 1.75 mW, Integration time: 10s]	59
A.6	Raman spectra of MB droplets in different concentrations after baseline correction (Only five spectra are plotted for better clarity). [Objective lens in use: 20x, Excitation wavelength: 532 nm, Power at sample: 1.75 mW, Integration time: 10s]	60
A.7	Raman spectra of MB aqueous solutions in the aluminium structure in different concentrations after baseline correction (Only five spectra are plotted for better clarity). [Objective lens in use: 50x, Excitation wavelength: 532 nm, Power at sample: 1.75 mW, Integration time: 10s]	61
A.8	Raman spectra of MB aqueous solutions in the aluminium structure in different concentrations after baseline correction (Only five spectra are plotted for better clarity). [Objective lens in use: 20x, Excitation wavelength: 532 nm, Power at sample: 1.75 mW, Integration time: 10s]	62
A.9	Raman spectra of Acetonitrile/ H_2O) = 1:1 solution in the aluminium structure obtained using the 5x, 20x, and 50x objective lenses (Excitation wavelength: 532 nm, Power at sample: 1.5 mW, Exposure time: 10s, Baseline is set to zero).	63
A.10	Raman spectrum of Carbaryl powder on the silicon surface before baseline correction (Objective lens in use: 5x, Excitation wavelength: 532 nm, Power at sample: 17 mW, Exposure time: 60s).	64
A.11	Raman spectrum of Dimethoate powder on the silicon surface before baseline correction (Objective lens in use: 5x, Excitation wavelength: 532 nm, Power at sample: 17 mW, Exposure time: 60s).	64

List of Tables

3.1	Experimentally observed vs. reported MB aqueous solution Raman peaks and their theoretical assignments.	18
4.1	Numerical aperture (NA) and solid angle of the light collection cone of different objective lenses.	29
4.2	Error estimation of the analytical model (calibration curve) predicting MB concentration in droplet samples using the 50x objective lens. Calibration curve equation: $y=75.002x+629.5$	46
4.3	Error estimation of the analytical model (calibration curve) predicting MB concentration in droplet samples using the 20x objective lens. Calibration curve equation: $y=118.18x+968.35$	47
4.4	Error estimation of the analytical model (calibration curve) predicting the concentration of MB aqueous solutions in the Al structure using the 50x objective lens. Calibration curve equation: $y=227.2x+4659.5$	48
4.5	Error estimation of the analytical model (calibration curve) predicting the concentration of MB aqueous solutions in the Al structure using the 20x objective lens. Calibration curve equation: $y=203.39x+1482.2$	49
4.6	Summary of the quantitative analysis of MB droplets and MB solutions in the Al structure.	50
4.7	Reduction in the LOD and LOQ of MB and the error of the analytical models by changing the sample configuration from MB droplets to MB solutions in the Al structure.	50

1

Introduction

1.1 Raman spectroscopy technique

Since the discovery of the Raman effect by C. V. Raman in 1928 [1], Raman spectroscopy has developed into a powerful technique in the field of rotational-vibrational spectroscopy. It is based on inelastic scattering of monochromatic light from molecules that is accompanied by a change in the vibrational or rotational energy of a molecule and thus also a change in frequency of the radiation. Each molecule has a very specific rotational-vibrational spectrum, and therefore a specific spectral fingerprint by which the molecular composition can unambiguously be identified.

In recent years, Raman spectroscopy has had promising results in applications ranging from the rapid identification of unknown substances to the detailed characterisation of various materials. In fact, the sensitivity of this technique to small changes in the material structure, its ability to noninvasively analyse different samples and to analyse samples in aqueous solutions with minimal interference from water have drawn a lot of attention to apply it in a range of different fields. Whether the objective is a qualitative or quantitative analysis, Raman spectroscopy is capable of providing key information very quick. However, despite these outstanding features, some problems and challenges remain.

1.2 Motivation of the research

A variety of spectroscopic techniques have been used for material and/or structural identifications [2–4]. Among them, Raman spectroscopy has opened up many new applications in the field of molecular spectroscopy. Compared with other common molecular spectroscopic techniques, like Fourier Transform Infrared (FTIR) and Near Infrared (NIR) spectroscopy, Raman combines the high spectral information content of FTIR with the sampling simplicity of NIR. This makes Raman spectroscopy a well-suited and widely-used technique to identify and also to quantify molecular constituents in liquid, gas and solid samples.

Moreover, advantages of Raman spectroscopy such as flexible and non-invasive sampling and its general compatibility with fibre optics make it a very suitable method to be used for remote sensing, which is the main objective of our future work. However, qualitative and quantitative fibre-optic Raman spectroscopy are challenging and require a careful understanding and control of all experimental parameters, including laser excitation power and wavelength, sample properties, measurement reproducibility, fibre coupling efficiency etc.

The above-mentioned challenges in fibre optic Raman spectroscopy provide a motivation to investigate how different experimental factors can affect measured Raman signals. That way, one can control and modify experimental parameters with the aim to provide optimised experimental conditions under which best results can be achieved. Therefore, in this study, we explore the performance of conventional Raman spectroscopy, which is preferable in remote sensing, for the analysis of a specific molecule under different experimental conditions including different material phases, laser spot size, power, wavelength etc.

Besides operational factors that can influence the recorded data, Raman spectroscopic limits of detection (LOD) are needed for the evaluation of the results. The question therefore arises how one might calculate and decrease the LOD of a given substance using Raman spectroscopy. Thus, another important motivation for this research is to apply suitable methods for the calculation and minimisation of the LOD of our analyte by exploring experimental parameters that influence this important quantity.

So far, the use of Raman spectroscopy for quantitative analysis has not kept pace with its use for qualitative analysis. In fact, the difference in Raman cross section for different species, different laser spot sizes, inhomogeneities, etc., can affect the quantitative analysis by Raman spectroscopy and make it challenging [5]. However, the development of quantitative Raman spectroscopy has the great potential to significantly improve the detection and the control of any changes in a given species since a modification of the chemical composition of a substance is normally reflected in its Raman spectra. Therefore, establishing an analytical model and

finding a mathematical relationship between a certain feature that can be extracted from a Raman spectrum and a targeted property, such as the analyte concentration, can be very helpful in many applications. Besides, the error of the analytical model should be calculated in order to assess the reliability of that model. Thus, other motivations of this research are to establish an analytical model for specific probe molecules using Raman spectroscopy, to estimate the error of prediction and to provide guidelines to minimise this error.

Finally, its specific features and its biological [6] and industrial importance motivated us to choose Methylene Blue (MB) as our probe molecule. It is also widely used in industry and in household products. The presence of MB in wastewater can restrict sunlight penetration into watercourses and is also harmful to humans due to its toxicity. Hence, in recent years, developing a fast and simple method to detect this dye, especially in solutions, has drawn much attention from both, an environmental as well as a scientific standpoint [7, 8].

1.3 Research framework and objectives

This nine-month Master of Research project has been started in July 2015 and has been carried out within the Department of Physics and Astronomy, Faculty of Science and Engineering at Macquarie University in Sydney, Australia. Based on Macquarie University's guidelines, the main body of this thesis must not exceed 55 pages. The work is fully funded by an international Research Training Pathway scholarship (iRTP) award.

The main objectives of this research work were:

- (1) To investigate the effects of changes in the excitation and collection optics, sample and instrumental parameters on the quality of the Raman spectrum of a given analyte.
- (2) To investigate the potential of Raman spectroscopy for quantitative analysis of a specific probe molecule, in our case MB.
- (3) To apply proper methods for the calculation of the limit of detection and quantification (LOD and LOQ) of MB by Raman spectroscopy under different experimental conditions.
- (4) To perform a systematic sequence of experiments and evaluate the results in order to modify the experimental conditions with the aim to minimise the experimental errors and the limit of detection and quantification (LOD and LOQ) of MB.
- (5) To develop an analytical model to predict the MB concentration in an unknown MB aqueous solution and estimate the error of prediction.

1.4 Thesis overview and contributions

This thesis consists of five chapters. The first chapter includes this introduction while the second chapter reviews the necessary background in the field of Raman spectroscopy.

In chapter 3, the instruments and methods used are presented. Different parts of our Renishaw Raman spectrometer as well as methods used for sample preparation are presented, and signal processing and data analysis techniques are discussed.

Chapter 4 contains our main experimental results followed by a detailed discussion. In the beginning, the choice of proper excitation wavelength and power are discussed. Then, in order to provide a general overview of the performance of our collection system, Raman spectra of a pure silicon wafer (our reference material) are collected using different objective lenses. Next, solid MB samples in powder form and MB droplets dried on the silicon wafer are studied. The efficiency of chemical activation of the silicon wafer to provide a uniform distribution of MB molecules and the performance of different objective lenses are evaluated in this regard. After that, Raman spectra obtained from MB aqueous solutions in droplet form are investigated. The suitability and efficiency of different objective lenses for quantitative analysis on MB droplets are investigated and the LOD and LOQ of MB droplets are calculated. Then, in order to improve the results, an aluminium structure that can be used as a modified sample holder is introduced. The experiments are repeated with the MB aqueous solutions constrained within the aluminium structure. The LOD and LOQ of MB are calculated and results are compared to the results obtained by MB droplet samples. Afterwards, based on the LOQ, new calibration curves that can be applied for predicting unknown MB concentration in aqueous solutions are developed. Then, to evaluate the reliability of our analytical models, the errors of these models are calculated. Eventually, results of different experiments are compared to find the optimum conditions for a quantitative analysis of MB.

The results of this work have been presented in:

- ● Mahdiah Dashtbani Moghari, Ewa Goldys, Alex Fuerbach, "*Optimal experimental conditions for minimising the limit of detection of Methylene blue by normal Raman spectroscopy*" - 24th Australian Conference on Microscopy and Microanalysis (ACMM24) - Feb 2016.

This work was awarded an Australian Microscopy and Microanalysis society (AMMS) bursary covering registration fee and travel expenses to attend ACMM24 conference.

- ● Mahdiah Dashtbani Moghari, Ewa Goldys, Alex Fuerbach, "*Quantification of Methylene Blue using normal Raman spectroscopy under different experimental conditions*" - Biofocus Research Conference - Dec 2015.

Finally, the thesis closes with a conclusion and a description of our planned future work.

2

Background

This chapter will provide a theoretical overview of the Raman effect and will discuss the key advantages and limitations of Raman spectroscopy. In addition, the basic principles of qualitative and quantitative analysis by Raman spectroscopy will be presented. Finally, the definition and importance of the quantities Limit of Detection (LOD) and Limit of Quantification (LOQ) and their differences will be described in this chapter.

2.1 The Raman effect

Raman scattering or the Raman effect was discovered by C. V. Raman in 1928 [1]. It is a fundamental process in which energy is exchanged between light and matter. When a sample is irradiated by a laser, light can be scattered or absorbed. The frequency of most of the scattered light is same as that of the incident light. This elastic scattering is called Rayleigh scattering. However, a small fraction of the light (approximately 1 in 10^7 photons) is scattered at frequencies that are different from that of the incident light. The process leading to this inelastic scattering is known as the Raman effect [9]. The Raman effect can be described in a classical or a quantum mechanical framework.

In a classical framework, light is considered as electromagnetic radiation containing an

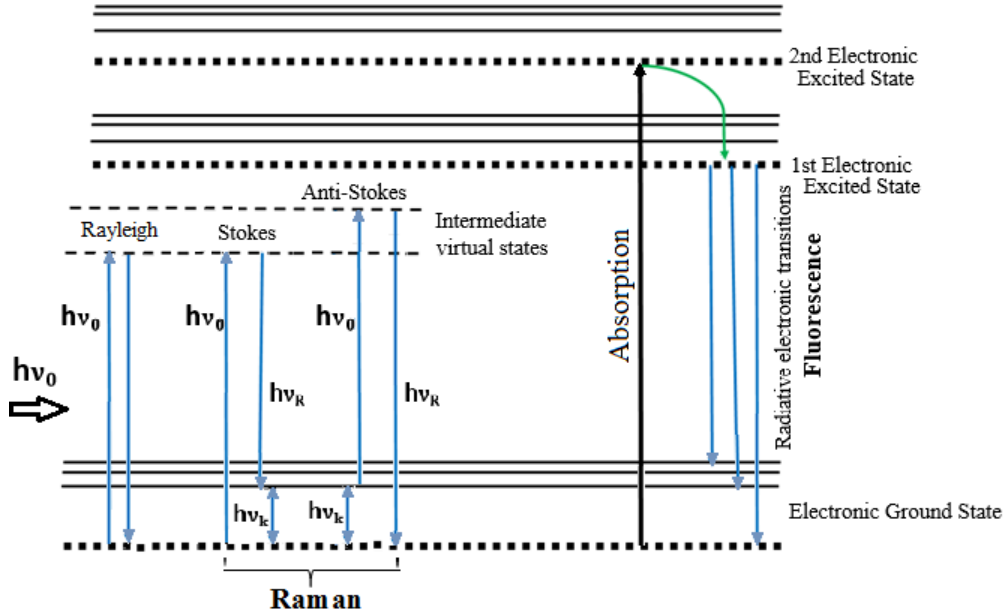


FIGURE 2.1: Molecular energy diagram showing Rayleigh and Raman (Stokes and anti-Stokes) scattering as well as fluorescence. ν_0 , ν_R and ν_k are the frequencies of the incident light, the Raman-scattered light and the molecular vibration (Raman shift), respectively.

oscillating electric field. When a molecule is put into an electric field, the electric field induces an electric dipole moment in the molecule which is described by [10]:

$$P = \alpha E \quad (2.1)$$

where P is the dipole moment induced in a molecule, E is the external electric field, and α is the polarizability of the molecule. The polarizability is a measure of how easy the electron cloud around a molecule can be distorted. For Raman scattering to occur, a molecular vibration must change the polarizability, either in magnitude, shape or direction during the vibration [10]. This change is described by the derivative of the polarizability, $\frac{d\alpha}{dQ}$, where Q is the normal coordinate of the vibration. Therefore, in order for a vibrational mode of the molecule to be Raman-active, the condition $\frac{d\alpha}{dQ} \neq 0$ must be fulfilled during the vibration.

From a quantum mechanical standpoint, light consists of photons which collide with the molecules and the Raman effect occurs when some photons are inelastically scattered after striking the molecule. In fact, in the process of Raman scattering a molecule is excited from its ground state to an excited or a virtual vibrational state, which is accompanied by the simultaneous absorption of an incident photon and the emission of a Raman scattered photon [9]. When the frequency of the scattered light is lower than the frequency of the incident laser (ν_0), the molecule remains in a higher vibrationally excited state ($m > n$ for the transition $n \Rightarrow m$). This process is called Stokes scattering, whereas anti-Stokes scattering, usually very weak, refers to $m < n$. Both processes are shown in Fig. 2.1.

2.2 Raman spectroscopy

Spectroscopy is the study of the interaction between electromagnetic radiation and matter. By analysing the light that is reflected, scattered or absorbed by a certain material, one can gain information about the physical, optical and molecular properties of that sample.

Raman spectroscopy is a fundamental form of molecular spectroscopy [11] and measures and analyses Raman scattered radiation from a sample. In Raman spectroscopy a sample is excited by a monochromatic laser with wavelengths either in the near infrared (NIR), visible or ultraviolet (UV) region. A rotational-vibrational Raman spectrum of the probe molecules is obtained by collecting the inelastically scattered light by a spectrometer and displaying it as a spectrum. The frequency difference between the incident and the Raman-scattered light is called the Raman shift, which is typically displayed as cm^{-1} . In a Raman spectrum, the intensity of the inelastically scattered light is displayed versus the Raman shifts. Since each molecule present in a sample has its own characteristic set of nuclear rotations and vibrations, the sample as a whole has a unique Raman signature. In fact, the Raman spectrum of a particular species consists of a series of characteristic peaks or bands shifted by one of the characteristic vibrational or rotational frequencies of that molecule [12]. These characteristic peaks are defined by their frequencies, shapes, and intensities. Analysing these properties reveals important information about the chemical structure and composition of the sample of interest [12–16].

2.3 Comparing Raman spectroscopy with infrared spectroscopy

Another common molecular spectroscopic technique is infrared (IR) spectroscopy, including Fourier transform infrared (FTIR) and Near-infrared (NIR) spectroscopy. It is based on the absorption of light by molecular vibration or rotation levels, whereas Raman spectroscopy is based on the inelastic scattering of light by those molecules. Similar to the Raman spectrum, the IR spectrum is unique for each molecule and reflects its molecular structure. Generally, Raman and IR spectroscopy are complementary to each other: if a chemical bond is covalent, its vibration modes are highly Raman-active and if the chemical bond is ionic, the vibration modes exhibit strong absorption in IR [10].

In this study, we use Raman spectroscopy since the challenges associated with FTIR

and NIR make them less suitable for our planned future work. In the case of FTIR, mid-IR light is necessary for FTIR absorption. This causes some problems with using this technique for remote sensing purposes since mid-IR light cannot be transmitted through standard optical fibres for more than a few meters. Moreover, mid-IR light does not penetrate many materials, which restricts sample flexibility in FTIR. Moreover, destructive sample preparation is needed in many cases and due to strong absorption of mid-IR light by water, water is an interfering factor in the study of aqueous solutions using FTIR. In the case of NIR, shorter wavelength light compared to FTIR is used. This makes NIR suitable for remote sampling, improves sample flexibility and causes less interference from water in the study of aqueous solutions. However, the main problem with applying NIR is that the NIR spectrum is not as information-rich as the FTIR spectrum for the same probe molecule.

Not only is a Raman spectrum information-rich, but it also does not have the disadvantages of the FTIR technique. This makes Raman spectroscopy a very attractive technique to be used for chemical analysis and monitoring. However, there are also some challenges with applying this technique, which have to be considered when designing an experiment. In the next sections, the main advantages and challenges of Raman spectroscopy will be discussed.

2.4 Advantages of Raman spectroscopy

Raman spectroscopy is a powerful technique and there are many advantages in applying it over other analytical techniques. Some of the key Raman advantages are as follows:

(1) Remote analysis: Optical fibres can be used to transmit laser light and Raman scattered light over hundreds of meters for remote analysis. Therefore, Raman is a suitable technique meeting the needs of our future work, which is the remote analysis of different samples.

(2) No or minimal sample preparation: Raman spectra can be obtained from samples with no or very little preparation [17]. In contrast, many other optical analytical techniques, such as IR spectroscopy, require sample preparation such as dissolution, grinding, or pressing. This feature of Raman spectroscopy makes it a very attractive technique to be used for remote analysis of different samples.

(3) Water is a weak Raman scatterer: Unlike other optical techniques like FTIR, Raman measurements are not influenced by the presence of water. Therefore, this technique can be used to analyse aqueous solutions and also biological samples in their natural environment without suffering from the large water absorption effects common with FTIR

technique [17]. We use this advantage of Raman spectroscopy to analyse aqueous solutions of Methylene Blue (MB) in this work and also for the remote analysis of chemicals in water which is planned in our future work.

(4) Non-destructive: If laser power and spot size are controlled, Raman spectroscopy is a non-destructive way to characterise materials. For example, it is possible to sample a solid inside a glass container without removing the solid.

(5) Detailed information: In addition to the material identification, further information such as crystallinity, phase, intrinsic stress or strain, concentration of a specific molecule in the sample and etc. about the sample under study can be achieved by analysing Raman spectra.

(6) Speed: Raman spectra can be acquired very quickly, within a few seconds. Moreover, the availability of extensive Raman spectral databases makes fast identification of unknown materials possible.

(7) In vivo and in situ analysis: Since laser light can be delivered and Raman scattered light can be collected quickly via optical fibres, which can be incorporated into catheters, endoscopes, cannulas and needles, as necessary, Raman spectroscopy can be carried out in vivo and in real time. Moreover, this technique is non-destructive and non-contact and is suitable for in situ analysis.

2.5 Challenges of Raman spectroscopy and some possible solutions

There are some challenges related to Raman spectroscopy. These challenges need to be known in order to be able to take measures to avoid or reduce their effects in experiments. Some of the main challenges and possible solutions to reduce them are outlined below:

(1) Fluorescence: When a sample is illuminated by a laser, both fluorescence and Raman scattering can occur. Fluorescence is an incoherent absorption-emission sequence, while Raman scattering is a coherent absorption-emission process. As illustrated in Fig. 2.1, fluorescence is a consequence of absorption of light by a molecule, which causes transfer of an electron to higher level of energy, i.e. an excited state. Then, this initially excited electron can change its state before it spontaneously emits light, which destroys the coherent nature of the process. The effect of fluorescence can be many orders of magnitude stronger than that of Raman scattering and the Raman spectrum can be partly or completely hidden due to

fluorescence. However, there are some methods that can be used to reduce or avoid unwanted fluorescence emission such as: changing the laser excitation wavelength (typically to a longer one), using a pulsed laser and time-resolved detection [18], photo-bleaching [19], baseline correction, shifting and subtraction of two Raman spectra collected at slightly different laser wavelengths [20], using a confocal setup [21], purification of the sample, and enhancement of Raman signals by Resonance Raman (RR) or Surface-Enhanced Raman Scattering (SERS). However, each of these methods comes with their own limitations and the proper method has to be applied under consideration of sample properties and experimental conditions.

(2) Sample heating: Radiating the sample with intense laser power can destroy the sample or cover the Raman spectrum. In a micro-Raman spectroscopy system, a laser power of few milliwatts is typically focused to a spot diameter of several micrometres, leading to high power densities of excitation and resulting in high local temperatures [22]. A high local temperature can induce crystalline changes and even melting of the sample [23, 24]. Therefore, these heating effects can lead to misinterpretation of spectral data. There are some techniques to avoid this phenomenon such as changing the laser wavelength, defocusing the laser beam on the sample, diluting the sample concentration to avoid absorption by the sample, cooling the sample, rotating the sample, rotating or oscillating the laser beam on a fixed sample, and reduction of laser power.

(3) The Raman effect is weak: Most of the light that scatters off the sample is unchanged in energy (Rayleigh-scattered) and only a small fraction-maybe 1 part in 10 million-has lost or gained energy (Raman-scattered). Thus, the Raman effect is intrinsically a weak effect. This problem can be addressed by sensitive and highly optimised instrumentation or by applying techniques like SERS where the intensity of Raman signals is enhanced by placing the probe substance on metal-nanostructured substrates or rough metal surfaces [25–27]. The SERS enhancement process is not fully understood yet, but it is generally accepted that it has two contributions: one is based on an electromagnetic effect and includes the enhancement of the incident electromagnetic field by surface plasmon resonances induced by the laser light in metallic nanoparticles [28]. The term "plasmon resonances" refers to a family of effects related to the interaction of electromagnetic radiation with metals. A description of the different aspects of plasmon resonances and the way they influence the SERS phenomena are given in [29]. The second contribution is based on a chemical effect related to chemisorption and encompasses either molecule-metal or metal-molecule charge transfers or chemical bond formations between metal surface and probe molecules [30]. However, there are some challenges in applying the SERS technique: Reproducing

a SERS substrate is challenging since the SERS signal intensities are related to the size [31, 32], shape [33–35], and distributions of the nanostructures on the substrate [36–38]. In addition, probe/metal interactions [29], difficulties of electrochemical studies in SERS for practical applications [29] and a dependence of the SERS technique to laser wavelength [29] can be problematic and need to be addressed when applying SERS. Finally, for remote sensing purposes, the development of sensitive and highly optimised instrumentation and the application of software-based discrimination techniques in spectral analysis have been suggested in the past [52, 53].

2.6 Qualitative vs. Quantitative Raman

There are two classes of measurements usually done by Raman spectroscopy: qualitative and quantitative analysis. Qualitative Raman measurements are based on extracting information about the chemical composition and functional groups present in a sample from its Raman spectrum. Most of quantitative Raman measurements are based on the proportionality of individual Raman peak intensities to the concentration of a particular species in a sample and allow measurement, monitoring, and controlling of the concentration of such species in a given sample.

2.6.1 Qualitative analysis by Raman spectroscopy

A Raman spectrum of a sample can provide detailed information about the molecules within the sample [41]:

- (1) The Raman shift, i.e. the location of characteristic Raman peaks in a spectrum is related to the vibration or rotation of a specific chemical bond or a single functional group in the molecule. It depends on the mass of the atoms and the strength of the chemical bonds between them. In fact, light atoms and strong bonds correspond to large Raman shifts, whereas heavy atoms and weak bonds are associated with small Raman shifts.
- (2) The polarization properties of a Raman peak are associated with crystal symmetry and orientation.
- (3) The width of a Raman peak can be an indicator of the quality of a crystal.

The combination of different Raman peaks and their relative intensities are unique in the Raman spectrum of a sample and can be used as a fingerprint for identification of the molecular structure/composition within a sample. Moreover, individual changes in the Raman spectrum can be an indicator of any changes in the sample. For instance, changes

in the frequency of certain Raman peaks can be an indicator of stress/strain in the sample.

Molecules have fundamental (normal) modes of vibration by which each atom vibrates with the same frequency but different amplitudes. Hence, fundamental modes are characterised by these frequencies (given in cm^{-1}). Molecules that contain N atoms have $3N-5$ fundamental vibrational modes if they are linear, whereas nonlinear molecules have $3N-6$ fundamental modes. Generally, a vibration can be Raman-active, IR-active, or both. However, if a molecule has a center of symmetry, vibrations that are symmetric with respect to the center of symmetry are Raman-active but not IR-active, while those that are antisymmetric with respect to the center of symmetry are IR-active but not Raman-active [10].

The number of Raman shifts in a Raman spectrum may be different in different situations and experimental conditions. Typically, not all Raman-active modes can be observed in a Raman spectrum. Some of them may be obscured by neighbouring strong bands or others may be inherently too weak to be observed even if the theory allows them.

2.6.2 Quantitative analysis by Raman spectroscopy

The intensity of a Raman peak depends on the concentration, or more precisely the number of specific scatterers present within the sampled volume. The intensity of a specific Raman band of a particular analyte in an ideal (non-absorbing) system can be defined as [42]:

$$I = I_D N_D dz \beta \quad (2.2)$$

where I is the specific intensity of the Raman signal (in photons $cm^{-2} sr^{-1} s^{-1}$), I_D is the incident laser intensity (photons $cm^{-2} s^{-1}$), N_D is the density of scatterers (molecules cm^{-3}), dz is the path length of the laser in the sample or the spectrometer depth of field (cm, whichever is smaller), and β is the differential Raman cross-section equal to $\frac{d\sigma}{d\Omega}$ ($cm^2 molecule^{-1} sr^{-1}$), which includes only the solid angle component over which scattering will be detected. σ is the empirically determined Raman cross-section ($cm^2 molecule^{-1}$) of a particular vibrational mode, which is proportional to the probability of an incident photon to be scattered as a Raman-shifted photon with a specific Raman shift. σ includes Raman scattering in all directions (over the full solid angle of 4π) from the sample. Ω represents the solid angle of the collection optics (sr).

According to equation 2.2, if the illuminated area is $1 cm^2$, the intensity of a Raman peak is proportional to N_D , which is the number of scatterers per cm^3 . Therefore, the Raman peak intensity scattered off an illuminated area, A_D , is proportional to the number of illuminated molecules as monitored by the spectrometer ($N_D A_D dz$), or the concentration

of the substance. This is the basis for most of the quantitative analysis done by Raman spectroscopy [43]. Moreover, quantitative Raman analysis is based on the principle of linear superposition. In fact, the Raman spectrum of a general sample is the weighted sum of the Raman spectra of its individual components.

Quantitative Raman spectroscopy can be divided into two categories: uni- (and bi-variate) and multivariate analysis [42]. The difference between these two approaches is in the number of features (variables) or frequencies utilized to do quantitative analysis.

Univariate analysis uses one feature in the Raman spectrum, such as a peak height, while bivariate analysis applies two features, such as the ratio of two peak heights, to extract information. These approaches are simple and in many cases can provide sufficient information and reliable predictability [44]. However, in the case of overlapping peaks or complex spectra these methods are difficult to be applied. In such situations, employing multivariate analysis is beneficial.

Multivariate analysis uses many variables in the spectrum to do quantitative analysis. This method is more complex and misinterpretation of the data is more likely compared with uni- or bi-variate analysis. However, the capability of multivariate analysis being used for analysing several components in a sample at the same time while not being affected by overlapping peaks and the possibility for the prediction of components even in the presence of interferences are some of the advantages over uni- or bi-variate methods [42, 43]. Common multivariate methods used in Raman spectroscopy are partial least squares (PLS) and principal component analysis (PCA).

2.7 LOD and LOQ

When applying Raman spectroscopy and doing quantitative analysis, it is important to be aware of the limit of detection (LOD) and the limit of quantification (LOQ) of the analyte under study. LOD is the threshold of differentiating between random noise and useful information. In each experiment, it is important to calculate the LOD for the given type of sample, instrument, and approach. If the concentration of the analyte is below the LOD, it is not possible to determine whether a given sample contains a certain analyte or not. That means that LOD expresses the lowest concentration of an analyte in a sample that can reliably be distinguished from zero but not necessarily quantified under the stated experimental conditions [45]. However, LOQ is the smallest amount of an analyte in the sample which can quantitatively be determined with proper accuracy [46, 47]. Therefore, the LOQ may be equal to the LOD or higher than it, but it can never be lower [48].

3

Instrumentation, experimental and analysis methods

The accurate analysis and correct interpretation of results and measurements obtained by Raman spectroscopy require a good understanding of the instrumentation, sample characteristics, signal obtained and analysis methods. These insights are not only required for an unambiguous interpretation of the measured data and for identifying its integrity, accuracy and limitations, but also for identifying the most suitable method to perform the measurement. Therefore, this chapter provides information about the used instrumentation, the chosen sample, and techniques that were employed in the course of this research project.

3.1 Raman Spectrometer

In this work, all Raman spectra were collected using a Renishaw InVia confocal Raman microscope. This Raman system consists of six basic units:

- (1) Monochromatic light sources (lasers).
- (2) A microscope that focuses the light onto the sample and collects the light scattered off

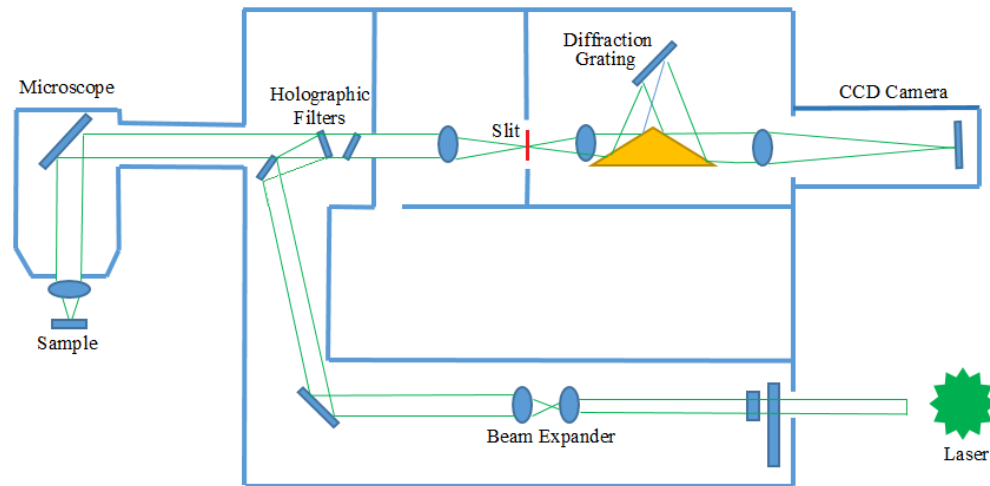


FIGURE 3.1: Schematic of the Renishaw InVia Raman spectrometer.

the sample.

(3) Holographic notch or dielectric edge filters which filter out all the light except for Raman scattered light. In fact, those filters block the Rayleigh-scattered light while transmitting both Stokes and anti-Stokes scattered light.

(4) A diffraction grating that splits the Raman scattered light into constituent wavelengths to provide a Raman spectrum.

(5) A thermoelectrically cooled, back-thinned, charge-coupled device (CCD) camera which detects the Raman scattered light.

(6) A computer that controls the instrument and also analyses the measured data.

A schematic and a photograph of our Renishaw InVia Raman spectrometer are shown in Fig. 3.1 and Fig. A.1 in the appendix, respectively. As shown in Fig. 3.1, the incident laser first passes through a beam expander which leaves the beam with a diameter that closely fills the back aperture of the microscope objective in order to deliver the smallest spot size to the sample. The beam is reflected off some mirrors to the first notch filter which reflects the beam to the microscope objective by which the beam is focused onto the sample. The scattered light that leaves the sample is then collected back through the same objective and passes the same path back to the spectrometer. It then passes through the notch filter which rejects Rayleigh-scattered light from reaching the spectrometer, while allowing the Raman-scattered light to pass to the spectrometer for analysis. The beam then passes through a second notch filter, which further rejects any Rayleigh-scattered light that might have passed through the first filter. The remaining light (the Raman signal) then passes through a lens

and is refocused onto the entrance slit of the spectrograph. The slit size can be adjusted in order to control the spectral resolution of the spectrometer. After passing through the slit, the light is reflected off a diffraction grating where it is separated into its respective wavelength components. The diffracted light is finally detected by a CCD camera. The CCD camera registers the output signal in counts, which is a measure of the photon flux at the detector [11]. Therefore, output Raman spectra are presented in terms of counts versus Raman shifts (cm^{-1}).

The system can operate in a static or extended configuration. If the static data collection setting is used, the grating is stationary while the light is dispersed onto the CCD. In the extended data collection setting, which we used in this study, the grating is rotated to collect a wider spectral range. In this configuration, the CCD data is read simultaneously with the grating rotation.

In the Renishaw confocal Raman spectrometer, the confocal nature of the collected data is provided by a two-step method: Firstly, a slit (Fig. 3.1) is used for spatial filtering of the collected signal in one direction. Secondly, filtering in the perpendicular direction is achieved by limiting the CCD detection area [49].

In our system, the excitation source is a continuous wave (CW) Nd:YAG laser (Samba model, Cobolt) which is internally frequency-doubled. It operates at a wavelength of 532 nm with a maximum output power of 50 mW. The Renishaw InVia confocal Raman microscope used for our experiments is coupled to a Leica DMLM microscope with 50x, 20x, and 5x objective lenses. The maximum measured power at the sample strongly depends on the microscope objective used. It is about 7 mW for the 50x, 14 mW for the 20x, and 17 mW for the 5x objective lenses. Data acquisition and spectrometer parameters are computer controlled and provided through the Renishaw WiRE 3.3 (Windows-based Raman Environment) software.

3.2 Methylene Blue

Methylene Blue (MB) is a cationic dye with a wide range of applications. It is greatly used as a potent drug for the treatments of many diseases [50]. Moreover, MB is extensively applied in industries and household products. However, the presence of MB in wastewater can limit penetrating sunlight into watercourses and is also toxic, which makes it dangerous to people. Therefore, in recent years, because of the biological and industrial importance of MB, developing a fast and simple method to detect this dye, specially in solutions, has drawn much attention [7, 8].

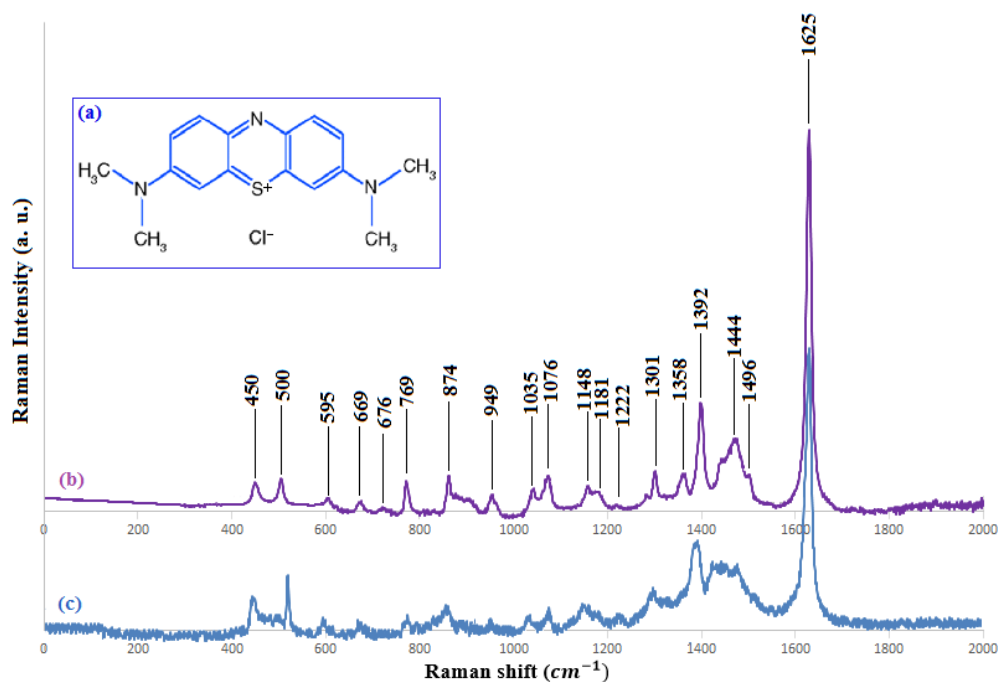


FIGURE 3.2: (a) Chemical structure of MB, Raman spectrum of (b) MB aqueous solution and (c) solid MB powder (Excitation wavelength: 532 nm, Power at sample: 1.75 mW, Exposure time: 10s).

Due to the above-mentioned reasons, MB was selected as the probe molecule in this study that aims at a quantitative analysis of MB using conventional Raman spectroscopy. Raman spectroscopy is a useful method for detecting organic dyes and SERS has been applied in many cases. Different methods such as spin coating [8], magnetron sputtering [51] and others have been applied for the fabrication of SERS substrates to enhance Raman scattering signals resulting in the detection of minuscule amount of MB. Although these methods have been successful in detecting very small amounts of MB, the problems that have been mentioned in section 2.5 with respect to the SERS technique still exist. Therefore, for remote sensing purposes, the development of sensitive and highly optimised instruments as well as of powerful software techniques or algorithms that can provide a set of discrimination techniques in the spectral analysis have been an area of considerable interest [52, 53].

Due to the above reasons, all Raman spectra presented in this study were acquired directly from MB molecules without applying the SERS technique. In fact, our aim was to find optimum experimental conditions under which LOD, LOQ, and the error of our measurements and analytical models became a minimum.

The structure of the MB molecule, the Raman spectra obtained in our lab from MB aqueous solution and MB powder are presented in Fig. 3.2. In Fig. 3.2(b) and (c), the Raman spectra of MB are shown for Raman shifts of up to 2000 cm⁻¹ since the fingerprint

Experimentally observed MB aqueous solution Raman peaks		
Reported MB Raman peaks [55]	Band assignment [55]	
450 (w)	$\alpha (C - N - C)_{AMG}$	
500 (w)	$\alpha (C - N - C)_{AMG}$	
596 (vw)	$\alpha (C - N - C)_{AMG}$	
669 (vw)	$\alpha (C - C - C)_{Ring}$	
676 (vvw)	$\gamma (C - H)_{Ring}$	
769 (w)	$\nu (C - H)_{Ring}$	
874 (w)	$\alpha (C - C - C)_{Ring}$	
948 (w)	$\rho (C-H_2); \beta(CH)$	
1035 (w)	$\beta (CH); \nu(C-S)$	
1078 (w)	$\beta (CH); \alpha (C - C - C)_{Ring}$	
1147 (w)	$\beta (CH)$	
1179 (vvw)	$\rho(C-H_3); \beta (CH)$	
1222 (vvw)	$\rho(C-H_3); \beta (CH)$	
1300 (w)	$\beta (CH); \nu (C - N)_{Ring}$	
1356 (w/sh)	$\nu (C - C)_{Ring}; \beta (CH)$	
1390 (s)	$\nu (C_9-N_{10}); \nu (C_3-N_2); \nu (C - N)_{Ring}; \beta(CH)$	
1445 (ms)	$\alpha (N - C - H)_{AMG}; \nu(C - C)_{Ring}; \nu(C - C)_{Ring}$	
1496 (w/sh)	$(CH_2)_{Twist}; \beta(CH)$	
1625 (vvs)	$[\nu(C - C)/\nu(C - N)]_{Ring}$	

vvs: very very strong; ms: medium strong, vvw: very very weak, vw: very weak, w/sh: weak shoulder
 ν : stretching; α, β : in-plane bending; γ : out-of-plane bending, ρ : rocking
 AMG: Attached to Methyl Group; Twist: Twisting

TABLE 3.1: Experimentally observed vs. reported MB aqueous solution Raman peaks and their theoretical assignments.

region of organic molecules is generally considered to be in the range from 500-2000 cm^{-1} [54]. As shown in Fig. 3.2, Raman spectra of MB aqueous solution and MB powder show excellent agreement indicating that there is no interference from the solvent (water) in our measurements.

The Raman spectrum of MB was obtained in the lab, and band assignments of its main features are listed in Table 3.1. Previously reported results [55] are also presented for comparison. In general, our results agree well with the previous reports.

3.3 Experimental procedure

The procedure that we followed in this study to apply Raman spectroscopy for the quantification of MB concentration includes four main stages:

Stage 1- Sample preparation: A series of standard solutions (i.e. solutions in which the MB concentration is accurately known) and a proper substrate, which is a chemically activated silicon wafer, are prepared.

Stage 2- Setup preparation: Before starting the experiment, a system calibration based on the silicon reference peak position at 520.5 cm^{-1} is performed and suitable values of laser



FIGURE 3.3: Block diagram of experimental procedure followed in this study.

power, objective lens magnification and laser exposure time are selected.

Stage 3- Signal processing: Signals are processed to extract suitable an accurate feature from the spectra for accurate MB quantification analysis.

Stage 4- Data analysis: Numerical data analysis is performed to calculate the LOD and LOQ of MB using Raman spectroscopy and to also calculate the error of the analytical models to investigate the suitability of Raman spectroscopy for quantitative analysis of MB concentrations.

These four stages are schematically shown in Fig. 3.3.

3.3.1 Sample preparation

In this study, aqueous solutions of MB with different concentrations were prepared. Moreover, in a part of this study, we chemically activated a silicon surface in order to evaluate the usefulness of this method to create a uniform pattern of MB molecules on the surface of the silicon wafer. The steps required for the preparation of MB solutions and the chemical activation of the silicon wafer are described in detail in the following sections.

MB aqueous solution preparation

MB ($C_{16}H_{18}ClN_3S \cdot 3H_2O$) was purchased from Sigma-Aldrich as a dark green powder with the molar weight of 373.90 g/mol. It is a water soluble powder and in solutions in water has a deep blue colour.

In order to make aqueous solutions of MB with different concentrations, firstly, a solution of high concentration of MB was prepared and then, diluted solutions were made from this stock solution. Therefore, we prepared an aqueous solution of MB with a high concentration of 0.0027 mol/L (Molar or M), equal to 2.7 mM or 1 g/L. To achieve that, we put a small piece of aluminium foil on an electronic analytical balance. The balance was zeroed with the aluminium foil on it. Then, MB was placed on the aluminium foil and accurately weighed. Afterward, a measurement cylinder was filled with deionized water to the required volume and the water was poured into the beaker containing the weighed MB powder. Finally, the solution was stirred with a magnetic stirrer to obtain a uniform solution.

To prepare fixed volumes of diluted solutions with specific concentrations from this stock solution, we applied the following equation [56]:

$$C_1V_1 = C_2V_2 \quad (3.1)$$

where C_1 is the concentration of the stock solution, V_1 is the volume of stock solution needed to make the new solution, C_2 is final concentration of new solution, and V_2 is final volume of new solution.

In this study, for simplicity, we consider the concentration of MB molecules in the stock solution (highest concentration solution, 2.7 mM), as 100%. Then, we can express the concentration of the dilutions as a percentage of the concentration of the stock solution. For example, 75% concentration refers to 2 mM solution since it is 0.75 of the concentration of MB molecules in the stock solution ($0.75 \times 2.7mM = 2mM$).

Chemical activation of silicon

Depositing a drop of MB aqueous solution on a silicon surface and leaving it to dry at room temperature in an air atmosphere leads to a non-uniform distribution of MB molecules over the surface of the silicon wafer after drying. This non-uniform pattern results from the so-called coffee-ring effect described by Deegan et al [57]. In fact, differential evaporation rates across the drop induce a capillary flow to the droplet perimeter to replenish liquid lost by evaporation near the edge. This edge-ward flow results in carrying additional solute to the edge and creating the coffee-ring effect.

MB is a cationic dye with an overall positive charge and dissociates in water into positively charged MB ions [58]. Therefore, a negatively charged substrate may be favourable for the adsorption of positively charged MB ions and reduce the radial flow of MB molecules to the droplet perimeter. In fact, electrostatic attractions between positively charged MB ions and a negatively charged substrate may result in reducing the coffee-ring effect.

In order to test if a negatively charged substrate was useful to reduce the coffee-ring effect and in creating a uniform pattern of MB molecules, we chemically activated a silicon surface to negatively charge it [59]: Firstly, we put the silicon wafer in a beaker and covered it with acetone. The beaker was then put in a sonicator for 15 minutes. Particles and contaminants that adhered to the silicon surface could be loosened as a result of the shaking and the silicon surface was cleaned. Then, the silicon wafer was placed in deionized water for 10 minutes. After taking the silicon wafer out of the deionized water, we left it in a mixture of 210 ml HCL (37%) and 90 ml H_2O_2 (30%) for two hours. Then, the silicon was thoroughly rinsed with deionized water. The above-mentioned process makes the silicon surface negatively

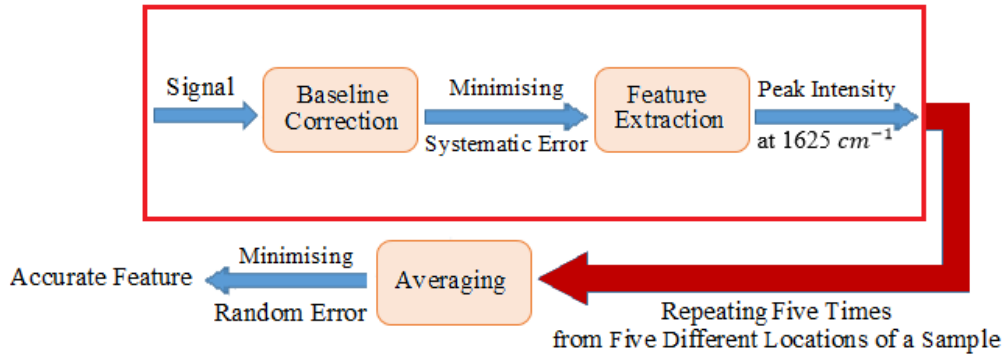


FIGURE 3.4: Block diagram of the signal processing steps that were followed in this study.

charged. In order to avoid discharging of the silicon surface, MB droplets with different concentrations were deposited on this substrate in less than 30 minutes and left to dry in air. Raman spectra were then obtained from these samples and the results are presented in section 4.3.

3.3.2 Setup preparation

In this study, as explained in detail later, we had to rely on a frequency-doubled Nd:YAG laser operating at the wavelength of 532 nm as excitation source.

The Raman system calibration and alignment were checked daily and whenever the system was powered on. Daily calibration of the wavenumber axis was achieved by recording the Raman spectrum of pure silicon by a 50x objective lens (one single accumulation, 10 seconds exposure time and 7 mW laser power incident on sample) in the extended configuration. Silicon has a known characteristic Raman peak that is located at 520.5 cm^{-1} . The position of this peak (in terms of CCD pixels) was correlated with the reference wavenumber value and this data was used to produce a calibration coefficient. The spectrometer software then calculated an accurate wavenumber scale to match system performance. Therefore, if necessary, an offset correction was performed to ensure the correct position of the silicon band at $520.50 \pm 0.1 \text{ cm}^{-1}$.

3.3.3 Raman spectra processing

In order to extract information from our measured Raman spectra, we needed to process the raw spectrum for each MB concentration. This process contained feature extraction and error minimisation. Feature extraction is extracting a specific signal property that we consider as our criterion to identify the concentration of MB, i.e. the height of a specific

Raman peak. Error minimisation is the process of minimising effects of unwanted signals originating from e.g. noise and fluorescence to obtain more accurate data.

The whole signal processing procedure applied in this study is shown in Fig. 3.4. Different parts of this figure are described in detail in the following sections.

Feature extraction

According to equation 2.2, the concentration of the probe molecule is proportional to its Raman peak intensities: As the MB concentration decreases, the intensity of its Raman characteristic peaks decreases. When we acquire Raman spectra from our samples, which are MB in solid state or MB aqueous solutions, we know that the observed signal originates from MB. Therefore, we can consider that the LOD of MB corresponds with the LOD of its most intense Raman peak, which is located at a Raman shift of 1625 cm^{-1} as can be seen in Fig. 3.2. Therefore, we can apply a univariate analysis using the MB peak intensity at 1625 cm^{-1} , which is assigned to (C-C) ring stretching and (C-N) ring stretching according to Table 3.1, as a criterion to estimate the MB concentration. Since the peak at 1625 cm^{-1} is the strongest MB Raman peak at the excitation wavelength of 532 nm, this peak is more detectable compared to the other MB Raman peaks in the diluted samples. Therefore, selecting this peak as our key feature leads to a very low LOD of MB.

Error minimisation

To enhance data accuracy, we need to know different sources of errors that affect the accuracy of our measurements and take effective measures to minimise their impact. All the experimental uncertainty is owing to either systematic or random errors [60].

Systematic errors and solution

Systematic errors are not determined by chance but are introduced by an inaccuracy inherent in the system. Systematic errors are often associated with a problem or flaw persisting throughout the entire experiment.

Systematic errors in our experiments were related to the baseline observed in the Raman spectra obtained from MB samples. It can be the result of fluorescence derived from MB molecules, thermal fluctuations on the CCD, effects of stray light, or the grain size distribution of the powder sample [61, 62]. During our experiments, we kept the light in the lab off and we also placed a cover around the sample under the microscope in order not to allow any interference from stray light such as the computer monitor. Therefore, it is less

likely that the baseline we observed in our Raman spectra was caused by stray light. Thus, the fluorescence originating from MB molecules or thermal fluctuations on the CCD can be probable factors that caused such baseline.

In this study, we applied mathematical methods to eliminate the baseline using MATLAB software and the intelligent fitting capability which is inbuilt in Renishaw's WiRE software. A spectrum before and after baseline correction is shown in Fig. A.2(a) and (b) in the appendix.

Random errors and solution

As opposed to systematic errors, random errors, as the name suggests, are random in nature and are errors in measurement caused by factors varying from one measurement to another. These errors may occur owing to the limitations in the accuracy of the measurement device or other factors beyond the control of the experimenter, such as experimenter's inability to take the same measurement in exactly the same way to get the exact same result or any changes in the measuring instruments or in the environmental conditions.

To achieve high accuracy, random errors need to be minimised. Random errors can be evaluated by statistical analysis and can be reduced by averaging over multiple measurements of the same quantity [63]. In fact, these kind of errors are completely random and scattered around the mean value, so it is expected that the average of them is zero. Therefore, in this research work, all values for our key feature, which is the Raman peak intensity at 1625 cm^{-1} , are obtained by averaging over five different measurements from five different locations at each sample to reduce random errors.

3.3.4 Data analysis

We need to analyse the data obtained to evaluate if it can be used for quantifying the MB concentration and for calculating the LOD of MB via Raman spectroscopy. Therefore, we calibrated our data and evaluated how well the data generated the calibration curves. If our data met the condition of equation 2.2 that is a linear relationship between Raman peak intensity and analyte concentration (in particular, a linear relationship between MB average Raman peak intensity at 1625 cm^{-1} and MB concentration), we calculated the LOD and LOQ of MB using the calibration curve. Then, we established a second calibration curve for MB concentrations equal to or higher than the LOQ to predict MB concentration and calculate the error of our analytical model.

Data calibration

We used curve-fitting to generate a mathematical model for the MB average Raman peak intensity at 1625 cm^{-1} vs. MB concentration. MATLAB software was used to apply the least squares method to find the best curve that would fit the data.

In practice, for each sample, the average peak intensity of the Raman band at 1625 cm^{-1} was used to define a calibration curve, i.e. a graph showing how the average peak intensity varies with the concentration. This calibration curve could then be used to analyse how well the measured data fitted the model. This is possible by using a criterion named goodness of fit. A good fit is a model in which the model coefficients can be estimated with little uncertainty and it is able to predict new observations with high certainty. The methods that are used to evaluate the goodness of fit fall into two groups [64]: numerical (or statistic) and graphical (or residual analysis). Computing goodness of fit statistics and coefficient confidence bounds yield numerical measures that aid statistical reasoning, while plotting residuals and prediction bounds are graphical methods that aid visual interpretation. In practice, we used both types to determine the best fit:

- **R-Square:** R-Square measures how well the fit explains the data variation. In other words, R-square is the square of the correlation between the response values and the predicted response values. The value of R-square is between 0 and 1. The higher the R-square, the better the model fits the data.
- **Plotting and analysing residuals:** The residual value is used for graphically evaluating the calibration curve to see whether the calibration curve fits the data strongly or not. The residuals from a fitted model are described as the differences between the response data and the fit to the response data at each predictor value:

$$\textit{Residual} = \textit{data} - \textit{fit} \tag{3.2}$$

If the model we fit the data with is correct, the residuals approximate the random errors. Thus, if the residuals behave randomly, the model fits the data well. However, if the residuals show a systematic pattern, it is an indicator that the model fits the data poorly.

LOD and LOQ calculation

As mentioned in section 3.3.3, we considered that the LOD of MB corresponded to the LOD of its strongest Raman band, which is Raman band at 1625 cm^{-1} , when excited by 532 nm

laser. There are different methods to calculate LOD and LOQ, among them visual definition and calculation from the signal-to-noise ratio (LOD and LOQ correspond to two or three and ten times the noise level, respectively) as well as linear regression are common ones [65].

In this study, we chose the linear regression method since the concentration of the probe molecule has a direct effect on the Raman peak intensity and a linear relationship between peak intensity and concentration is expected.

Linear regression

For a linear calibration curve, it is assumed that the instrument response y , is linearly related to the standard concentration x for a limited range of concentrations [65]. It can be expressed in a model such as:

$$y = ax + b \quad (3.3)$$

In this study, y is the MB Raman peak intensity at 1625 cm^{-1} and x is MB concentration. b is the slope of the calibration curve showing the sensitivity. This model is used to compute the sensitivity, b , and the LOD and LOQ. The LOD and LOQ can be calculated as [65]:

$$LOD = \frac{3S_a}{b} \quad (3.4)$$

$$LOQ = \frac{10S_a}{b} \quad (3.5)$$

where S_a is the standard deviation of the response. The standard deviation of the response can be estimated by the standard deviation of either y-residuals, or y-intercepts, of regression lines. This method can be used in all cases, but the background of signals should be set to zero. In this method a range of low values close to zero are used for the calibration curve, and a more homogeneous distribution will lead to a more pertinent assessment.

The standard deviation, S_a , is calculated by:

$$S_a = \sqrt{\frac{1}{n-2} \left[\sum (y - \bar{y})^2 - \frac{[\sum (x - \bar{x})(y - \bar{y})]^2}{\sum (x - \bar{x})^2} \right]} \quad (3.6)$$

where x and y are the actual concentration and the average Raman peak intensity at the concentration of x . \bar{x} and \bar{y} refer to the predicted concentration and predicted average Raman peak intensity estimated by the calibration curve. Moreover, n is the number of data point on the calibration curve.

4

Results and discussion

In this chapter, we present the results of our measurements using conventional Raman spectroscopy to investigate the suitability of this technique for quantitative analysis on MB molecules. In order to obtain clear results from our measurements, it is important to find optimum and reproducible experimental conditions under which strong and accurate signals can be obtained. Therefore, in this chapter, we present results from a systematic series of experiments on different forms of MB samples to investigate which factors can be modified to improve the results. Then, we implement those modifications in a new set of experiments and evaluate the improvements in the quality of our measurements.

In our experiments, optimum excitation wavelength, power, exposure time, objective lens, and sample configuration for an accurate and reproducible quantitative analysis on MB are studied. The LOD and LOQ of MB are calculated and the experimental conditions are modified until optimum results are obtained. Finally, analytical models that are capable of predicting the MB concentration are established and the errors in the prediction of the MB concentration under different experimental conditions are estimated and discussed.

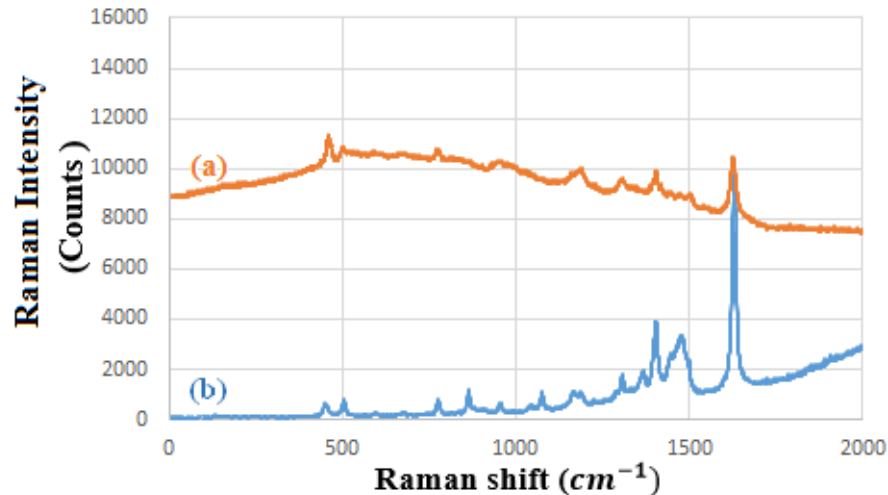


FIGURE 4.1: Normal Raman spectra of 100% MB aqueous solution in droplet from before baseline correction. The excitation wavelength is (a) 785 nm and (b) 532 nm (Objective lens used: 50x, Power at sample: 1.75 mW, Exposure time: 10s).

4.1 Selection of suitable excitation wavelength, exposure time, and laser power

***Excitation wavelength:** Our Renishaw Raman system is equipped with a frequency-doubled Nd:YAG laser and a diode laser operating at 532 nm and 785 nm, respectively. In this study, in all experiments, we used 532 nm as our excitation wavelength since higher quality Raman spectra with higher resolution could be recorded using this excitation wavelength. In fact, in the absence of resonance effects, shorter excitation wavelength increases the Raman cross section by the inverse fourth power of the laser wavelength, $\frac{1}{\lambda^4}$, which enhances Raman peak intensities and the signal-to-noise ratio (SNR) [66].

However, a shorter excitation wavelength is not always an ideal choice for Raman experiments. Decreasing excitation wavelength leads to an increase in the excitation photon energy and as a result, enhances the likelihood of sample damage/heating or fluorescence. However, these were not problematic in our experiments since sample damage was prevented by controlling the exposure time and power at the sample. Moreover, as shown in Fig. 4.1, switching to the longer wavelength laser, 785 nm, led to a relatively large background in the Raman spectra of MB. Therefore, we chose 532 nm as our excitation wavelength due to higher quality and SNR of the recorded Raman spectra of MB at this wavelength.

In addition, a comparison between the MB Raman spectra obtained using 785 nm and 532 nm excitation wavelength (Fig. 4.1) shows that both spectra agree with each other in

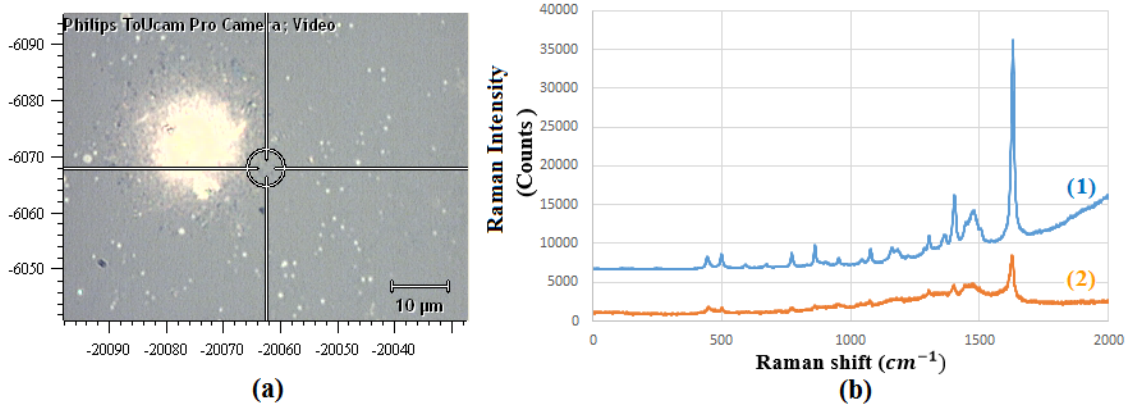


FIGURE 4.2: (a) Colour change of 100% MB aqueous solution from dark blue to yellow as a result of photochemical damage, (b) Normal Raman spectra of 100% MB aqueous solution: (1) before photobleaching (Objective lens in use: 50x, Excitation wavelength: 532 nm, Power at sample: 1.75 mW, Exposure time: 10s) and (2) after photobleaching (Objective lens in use: 50x, Excitation wavelength: 532 nm, Power at sample: 7 mW, Exposure time: 10s).

terms of the location of the characteristic Raman peaks of MB. This implies that the measured peaks are indeed MB Raman peaks and have not originated from noise.

***Exposure time and excitation power:** According to equation 2.2, the Raman peak intensity increases as incident power density, I_D , increases. However, a high laser power density usually causes some thermal or photochemical damage to the sample. MB, in particular, can be photobleached if irradiated by a laser of high power for relatively long time. Photobleaching is a dynamic process during which fluorochrome molecules undergo photo-induced chemical damage and covalent modification upon exposure to the excitation light [19]. Photobleaching causes sample damage, reduction of the peak intensities, and alteration of the relative heights of Raman peaks of the specimen, which are not favourable [67, 68].

Fig. 4.2 (a) shows colour changes in a MB aqueous solution from blue to yellow after photobleaching. Moreover, a reduction in the MB Raman peak intensities due to photochemical damage and photobleaching are shown in Fig. 4.2 (b). Therefore, one has to take care to select the laser power that is high enough to obtain strong Raman peaks, yet low enough in order not to cause sample degradation.

Therefore, in order to prevent photo damage, the laser power at the sample needs to be optimised. This was done by considering the laser spot size provided by each objective lens applied in this study. The laser focal spot diameter, d , can be calculated by [69]:

$$d = \frac{1.22\lambda}{NA} \quad (4.1)$$

where NA is the effective numerical aperture, defining the spatial resolution as well as the collection efficiency, and λ is the excitation wavelength.

Objective lens	NA	Solid angle (sr)
50x	0.75	2.127
20x	0.4	0.525
5x	0.12	0.045

TABLE 4.1: Numerical aperture (NA) and solid angle of the light collection cone of different objective lenses.

According to the Table 4.1, among the objective lenses used in this study, the 50x objective has the largest NA. Hence, as equation 4.1 suggests, the smallest laser spot diameter is obtained using the 50x objective. For a given laser power at the sample, the highest power density results from using the objective lens that provides the smallest laser spot size, which is the 50x objective in our experiments. Thus, the chance of photobleaching is greatest when this objective lens is used. Therefore, we determined the optimum power at the sample (MB in aqueous solution) using the 50x objective. For that, for each MB concentration, we kept the exposure time (integration time) at a short time, 10 s, to prevent photobleaching and started recording MB Raman spectra for different laser powers, starting from the lowest. At each power level, we recorded the MB peak intensity at 1625 cm^{-1} and then increased the laser power until reaching the point at which increasing the power caused a reduction in peak intensity. At this point, photobleaching has occurred and we define this as the damage threshold of our sample. Therefore, the highest Raman peak intensity is obtained using a laser power level just below the damage threshold of the sample. This optimum laser power at the sample was 1.75 mW in our case, based on those results. In fact, our results further showed that for all MB samples with a concentration higher than 55%, a power higher than 1.75 mW at the sample caused a reduction in peak intensity. Therefore, we chose 1.75 mW power as the optimum power for the measurement of all MB samples with different concentrations.

It should be mentioned that in all our experiments, we kept the power at the sample the same rather than the power density. This is because in most Raman systems, the laser power can be controlled, rather than the power density. Moreover, the laser spot area, as calculated by equation 4.1, of the 5x objective is roughly 39 times bigger than that of the 50x objective. Thus, in order to achieve the same power density using the 50x and 5x objectives, the output power using the 5x objective should be 39 times higher than that using the 50x objective, i.e. 68 mW instead of 1.75 mW. However, as mentioned in section 3.1, this is impossible as the maximum power at the sample using the 5x objective is 17 mW in our Raman system. Moreover, our main interest is to find out how the Raman signal depends on the choice of objective lens for a given (limited) laser power. Therefore, during all experiments done by

using different objective lenses, we kept power at sample the same and set it to 1.75 mW.

***Other considerations:** Due to very short working distance of the 50x objective lens, which is only 0.5 mm, we adjusted the focus of the laser spot to lie on the top of the sample to avoid any contact between this objective lens and the sample. Therefore, in order to keep the experimental conditions constant, we always focused on the top of the sample when recording Raman spectra, also when using other objective lenses.

Moreover, in this chapter, to facilitate a clear comparison of the length of the error bars of different graphs used for calculating LOD and LOQ, the same vertical scale has been chosen for all such graphs. For the same reason, the vertical scale of the all graphs used for establishing analytical models are also the same. Moreover, for simplicity, we express the concentration of MB in the horizontal axis of all graphs in terms of percentage. In fact, we consider the concentration of the 2.7 mM MB aqueous solution as 100% and express the concentration of the dilutions as a percentage of this.

4.2 Reference System

Prior to the measurements on MB samples, we have established a reference to investigate the behaviour of our detection system. For that purpose, we used a silicon wafer as our test sample since it is an isotropic Raman scatterer and recorded its Raman spectra using different objective lenses. According to Table 4.1, different objective lenses have different solid angles indicating the collection cone by which scattered light is collected. Therefore, different objective lenses have different light collection efficiencies.

Fig. 4.3 shows the Raman peak intensity of silicon at 520.5 cm^{-1} versus the solid angle of the different objective lenses. The vertical error bars represent the variations of the silicon Raman peak intensity over five measurements from five different locations on the silicon wafer. According to Fig. 4.3, there is a linear relationship between silicon average Raman peak intensity and the collection cone of the objective lens ($R^2=0.9977$). Since silicon is opaque for visible light [70], the effective laser path length (dz) in equation 2.2 is limited by the sample opacity. Therefore, according to equation 2.2, only the incident laser intensity, the number of scattering molecules in the focus area and the differential Raman cross section are effective factors that determine the strength of the Raman peak intensity of silicon.

According to equation 4.1, a change in solid angle or NA of the objective lens results in a change in the spot size and thus the excitation area. The intensity of the incident laser is inversely proportional to the size of the excitation area, while the number of scattering

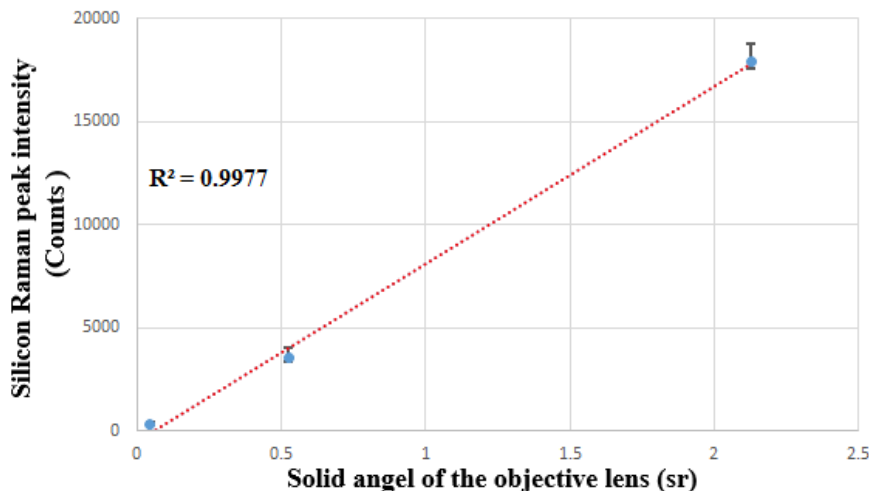


FIGURE 4.3: The intensity of the silicon Raman peak at 520.5 cm^{-1} vs. the solid angle of the microscope objectives in use while the excitation wavelength is 532 nm and the power at the sample is fixed at 1.75 mW . The vertical error bars show the peak intensity variations over five measurements from different locations of the silicon wafer and data points show the average peak intensity taken over five such measurements.

molecules is directly proportional to it. As a result, according to equation 2.2, changes in the incident laser intensity due to the different laser spot sizes are exactly offset by the variations in the number of scattering molecules present in the excitation area. In other words, the variations in the incident laser intensity and in the number of scattering molecules cancel each other out. Therefore, if everything else is equal, a change in the objective lens and thereby, the excitation area does not result in a net change of the total intensity of the Raman scattered light. Thus, the total Raman scattered intensity from the focus areas of 50x, 20x, and 5x objective lenses are the same. The objective lens that has a bigger collection cone (or a bigger NA) can collect more of the Raman signal, which leads to the stronger Raman peak intensity. Consequently, for planar, opaque and isotropic samples such as silicon, the efficiency of the objectives decreases from the 50x objective to the 5x objective.

Raman spectra of silicon wafer obtained using the 50x, 20x, and 5x objective lenses are also presented in Fig. A.3 in the appendix.

4.3 LOD of MB in solid-state form

To acquire Raman spectrum of MB in solid form, we have placed a very small amount of MB powder on a silicon wafer. We have sandwiched the MB powder between the silicon wafer and a glass slide in order to produce a very thin and flattened sample area on the silicon and then we recorded its Raman spectrum (Fig. 3.2(b)). Since the number of MB molecules cannot be controlled properly by this method, it is not a suitable method to be applied for

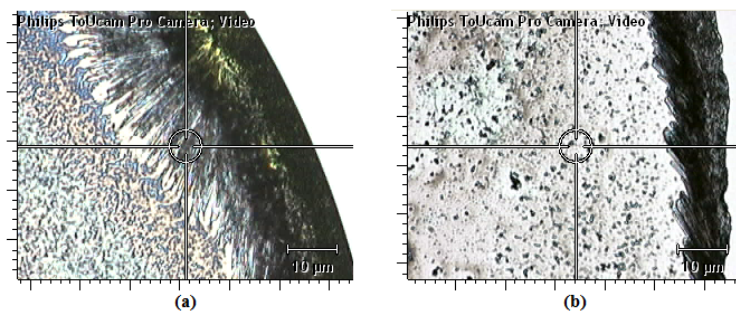


FIGURE 4.4: Coffee-ring effect of a MB droplet dried on a (a) regular silicon and (b) negatively charged silicon surface.

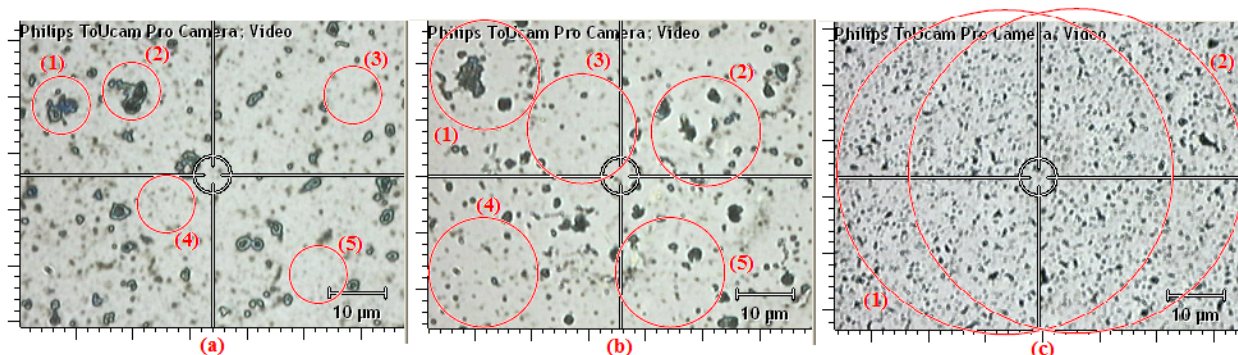


FIGURE 4.5: Sampling area of the (a) 50x, (b) 20x, and (c) 5x objective. In (a) and (b), the Raman peak intensities obtained from the (1) and (2) areas are much higher than those of the (3), (4), and (5) areas, while the spectral differences are negligible in the (1) and (2) areas of (c).

LOD studies.

As the next step, we dropped MB aqueous solutions on the silicon wafer and left them to dry in air. However, we could also not achieve a reliable quantitative analysis of such samples due to their inhomogeneity and the coffee-ring effect (described in section 3.3.1). Therefore, in an attempt to reduce the coffee-ring effect and to achieve an even distribution of MB molecules throughout the surface of silicon, we negatively charged the silicon surface by the method described in section 3.3.1. We then dropped an aqueous solutions of MB, containing MB ions with positive charge, on the surface of a negatively charged silicon wafer and left them to dry in an air atmosphere. Fig. 4.4(a) and (b) show the pattern of the edge of a MB droplet dried on a regular and a negatively charged silicon surface, respectively. These figures indicate that chemical activation of the silicon surface can not completely mitigate the coffee-ring effect, and is not a successful method to overcome this phenomenon.

Fig. 4.5(a), (b), and (c) show the images captured by the 50x, 20x and 5x objectives from the central part of a MB droplet dried on the negatively charged silicon surface. We collected the Raman spectra using the 50x, 20x, and 5x objectives from the central areas of this sample to explore and compare the performance of these objective lenses in the case of

sample inhomogeneity.

Results show that variations of the peak intensity acquired from different locations of the inhomogeneous sample are highest when the 50x objective is used. Due to inhomogeneity, spectra obtained from multiple locations of the same sample strongly depend on the location of the objective lens on the sample. According to equation 4.1 and considering Table 4.1, the laser spot diameters resulting from the 50x, 20x, and 5x objective lenses are $0.87 \mu\text{m}$, $1.62 \mu\text{m}$, and $5.41 \mu\text{m}$, respectively. The highest magnification and the smallest laser spot diameter are obtained by the 50x objective. Thus, this objective is more sensitive in terms of sample inhomogeneity since the number, size and the shape of MB molecular clusters are most evident at this magnification. However, for the 5x objective, the spectra are averaged over a large sample area and therefore, spatial differences are almost negligible using this objective.

In Fig. 4.5(a), (b), and (c) circles with a ratio of 1: 1.86 : 6.22 are drawn, corresponding to the laser spot diameters for the 50x, 20x, and 5x objectives. As can be seen in these figures, the variations of the Raman peak intensities collected from different spots of a sample decrease as the magnification of objective lens is reduced: The largest variations in peak height are observed for 50x objective, while the lowest peak variations are related to the 5x objective. The short length of the error bars in Fig. A.4 in the appendix also confirms the low variations in MB peak intensity obtained by the 5x objective from different locations on the sample. Plots for the 50x and 20x objectives are not shown due to the huge differences in peak intensities acquired from different points on the sample.

As mentioned before, in the case of inhomogeneity, Raman spectra are not truly representative of the number of MB molecules. That is, the abundance of MB molecules in the area of the sample illuminated by the laser spot is not characteristic of the entire sample. The problems with sampling heterogeneous materials is a principal limitation for quantitative analysis [71–73] and data acquired from such samples cannot be used for LOD studies and quantification of the sample concentration.

4.4 LOD of MB in aqueous solutions

In order to reduce inhomogeneity problems, we recorded Raman spectra directly from MB solutions. In fact, solutions are more homogeneous and mostly do not have the problems associated with variable particle sizes and shapes. We have recorded Raman spectra from MB aqueous solutions since measuring relatively strong Raman scatterer (MB) in the presence of weak Raman scatterer (water) is more straightforward. In fact, as Fig. 3.2 shows, Raman

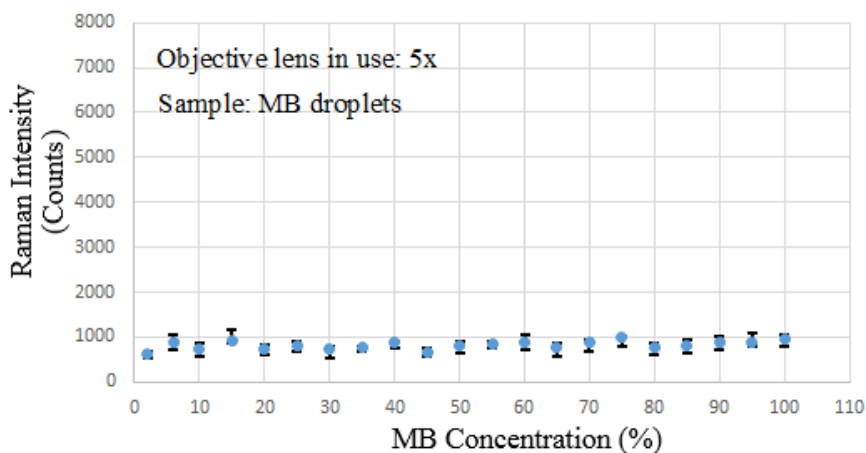


FIGURE 4.6: The intensity of the MB Raman peak at 1625 cm^{-1} vs. MB concentration obtained using the 5x objective lens from MB solutions in droplet forms (Excitation wavelength: 532 nm, Power at sample: 1.75 mW, Exposure time: 10s).

spectra of MB aqueous solution and MB powder agree well with each other, which indicates that water does not produce interfering Raman signals in our measurements.

4.4.1 LOD of MB in droplet samples

In this experiment, Raman spectra were acquired directly from MB aqueous solutions in droplet forms. For that, $20\ \mu\text{L}$ of freshly prepared MB aqueous solution in low concentration, prepared as described in section 3.3.1, was dropped onto the surface of a silicon wafer using a pipette. Raman spectra were then collected from five different locations on each sample. The spectra were baseline corrected with the baseline set to zero and intensities were recorded for the MB Raman peak at 1625 cm^{-1} , which is our selected signature feature as described in section 3.3.3. Results are shown in Figs. 4.6, 4.7, and 4.8. In all these figures, data points are an average of five measurements for the peak intensity at 1625 cm^{-1} per sample and the vertical error bars represent the variations in the peak intensity at 1625 cm^{-1} related to the specific concentration.

Evaluation of the performance of the 5x objective lens for MB droplet samples

As Fig. 4.6 shows, although the MB Raman peak at 1625 cm^{-1} is detectable when the 5x objective lens is used, the variations in the average peak intensities at 1625 cm^{-1} for different concentrations are scattered and show no obvious trend. Therefore, the 5x objective lens cannot be used to identify the concentration of MB. In fact, the 5x objective can be used for detecting MB, but it is not sensitive enough to be used for LOD and LOQ studies and quantitative analysis.

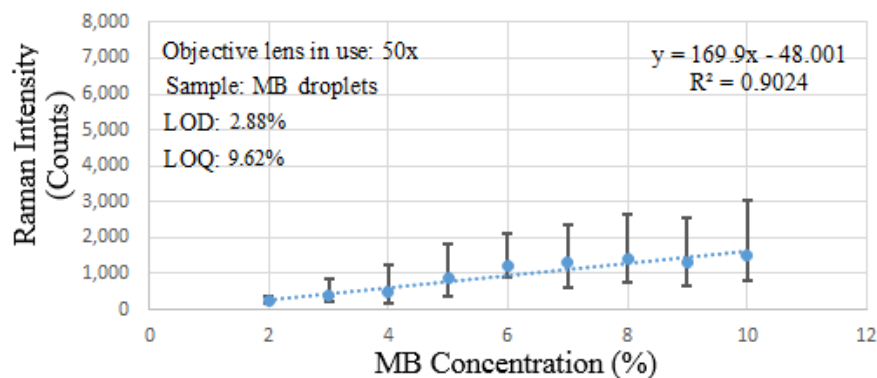


FIGURE 4.7: The intensity of the MB Raman peak at 1625 cm^{-1} vs. MB concentration obtained using the 50x objective lens from MB solutions in droplet forms (Excitation wavelength: 532 nm, Power at sample: 1.75 mW, Exposure time: 10s).

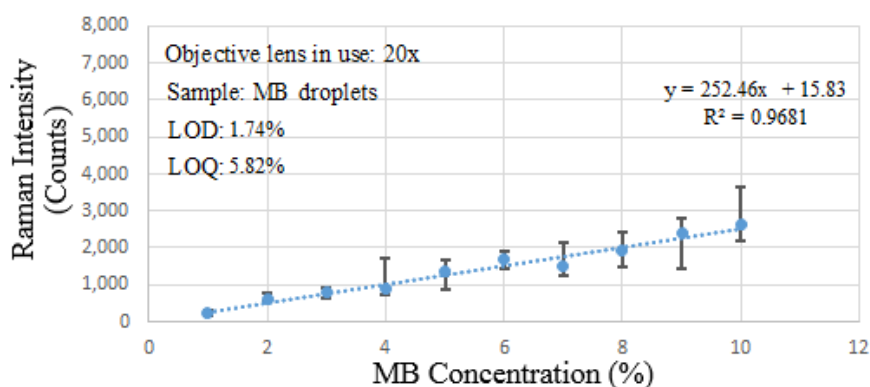


FIGURE 4.8: The intensity of the MB Raman peak at 1625 cm^{-1} vs. MB concentration obtained using the 20x objective lens from MB solutions in droplet forms (Excitation wavelength: 532 nm, Power at sample: 1.75 mW, Exposure time: 10s).

Evaluation of the performance of 50x and 20x objective lenses for MB droplet samples

As Figs. 4.7 and 4.8 show, when Raman spectra of MB droplets are obtained using the 50x and 20x objective lenses, R^2 values are close to one, which shows that the measurement can be fitted using a linear function. This linear relationship between the mean value of the Raman band intensity at 1625 cm^{-1} and the MB concentration is in agreement with equation 2.2. Therefore, the 50x and 20x objectives have acceptable sensitivities to be employed for LOD and LOQ studies and quantitative analysis on MB droplets.

A Comparison between Figs. 4.7 and 4.8 shows:

(1) In each specific concentration, a stronger average Raman peak intensity at 1625 cm^{-1} is acquired using the 20x objective compared to the 50x objective. However, when we obtained Raman spectra from the silicon sample (see Fig. 4.3), we found that the 50x objective was more efficient than the 20x objective. These different results originate from differences in

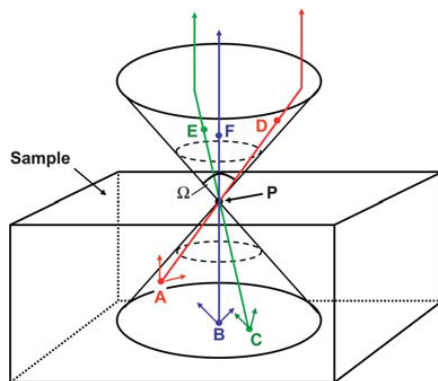


FIGURE 4.9: Schematic drawing demonstrating the origin of out-of-focus contributions to Raman signals. Photons originating at A, B and C which traverse paths APD, BPF and CPE will pass through P and thus through the confocal aperture. Summing all the similar contributions throughout the extended illumination volume leads to a non-negligible out-of-focus signal [74].

sample properties and configurations.

In the case of silicon, the effective path length of the laser in the sample is limited due to the sample opacity. Thus, an opaque sample such as silicon is considered as an optically thin sample. This makes the signal collection mechanism relatively straightforward. In fact, for the opaque samples, light is scattered from the region determined by the confocal pinhole on the sample and collected by the collection cone of the objective lens and there are almost no out-of-focus rays generated in the bulk of the sample.

However, in the case of thick transparent or lightly turbid samples, such as MB aqueous solutions, the excitation region of the sample and the signal collection mechanism become very complicated. For these samples, the sample thickness is much larger than the depth of field of the spectrometer. Thus, the path length of the laser in the sample is not limited in such samples. The excitation region is within the extended illumination volume of the sample and not just the surface of the sample. Moreover, there is an additional contribution to the light collected at the sample-air interface due to out-of-focus rays which find their way into the collection cone of the objective lens. That is, confocal pinhole arrangements do not work well for transparent or lightly turbid samples. In fact, for these samples, the out-of-plane signal rejection is relaxed due to the signals generated within the extended illumination cone [74–76].

As illustrated in Fig. 4.9 [74], for a transparent or lightly turbid sample, an extended volume is illuminated by the laser focused to a small spot labelled P. There is the probability that scattered rays generated at all points within this volume (and not just the paraxial rays), propagate towards the point P. Thus, if such rays fall within the acceptance cone of the lens and are collimated, they can make their way through the confocal pinhole. The probability

that an out-of-focus ray originating at a point C, passes through point P and is subsequently collimated, is small compared to the number of rays scattered from point C. However, if the total number of rays that meet the above conditions are integrated over the extended volume, they can provide a considerable contribution to the signal collected at point P. The lower the NA, the higher the impact of out-of-focus response will be [74]. Therefore, the impact of out-of-focus rays is higher for the 20x objective compared with the 50x objective.

The depth of focus or depth of field for such lightly turbid samples can be described as the distance between two points on either side of the focus, where the intensity of the beam falls to 0.5 of its maximum value and is given by [11]:

$$h = 2.53\lambda\left(\frac{f}{D}\right)^2 \quad (4.2)$$

where f is the focal length of the lens and D the effective beam diameter at the lens.

Moreover, the focal volume τ is approximately given by [11]:

$$\tau = 3.2\lambda^3\left(\frac{f}{D}\right)^4 \quad (4.3)$$

The ratio $\frac{f}{D}$ is closely related to the numerical aperture by [11]:

$$\frac{f}{D} = \frac{0.5}{\tan(\arcsin(NA))} \quad (4.4)$$

For the small values of NA: $\frac{f}{D} \sim \frac{1}{2NA}$. Hence, a larger NA corresponds to a smaller $\frac{f}{D}$ and as a result, according to equation 4.3, results in a smaller focal volume. Thus, the focal volume of a 50x objective is smaller than that of a 20x objective. In fact, the laser power coming out of a 50x objective is highly localised to a small focal volume and the quality of Raman signals highly depends on the scattered signals coming out of this small focal volume. Thus, this objective is more sensitive to the accuracy of the focus and if the sample is slightly out of focus, the collected Raman signals fall off rapidly. Due to the curvature shape of the droplet surface, finding the exact focus point on the MB droplet, specially when acquiring Raman signals using a 50x objective, is challenging. Since the 50x objective is more sensitive to the exact focus position, the Raman signals are reduced more as a result of inexact focussing compared to a 20x objective. However, due to the higher impact of out-of-focus response for the 20x objective, even in case of inexact focussing, there are still considerable scattered signals coming from out-of-focus regions. Therefore, the 20x objective lens is less sensitive to the exact focal point compared to the 50x objective.

Moreover, at a magnification as high as 50x, slight vibrations from an illuminator or computer fan can cause the video feed to dramatically shake and move in and out of focus. In addition,

the droplet itself can move out of focus since it is not surrounded or restricted and can vibrate or shake freely. Therefore, the focus point is less stable for a 50x objective compared to a 20x objective. In fact, a slight shake of the sample can lead to a change in focus position for the 50x objective and thus a further reduction in the collected signals.

In summary, compared to a 50x objective lens, factors such as a larger contribution of out-of-focus rays originating within the extended illuminated volume of a 20x objective, a smaller sensitivity to the focus point position, and a more stable focus can be considered as advantageous factors for measuring the Raman peak intensities of MB droplet samples using a 20x objective. However, the smaller collection cone of a 20x objective due to its lower NA is a reducing factor for the detection of Raman signals. The stronger average Raman peak intensity obtained by the 20x objective in each specific concentration indicates that the effects of advantageous factors are stronger than the effect of reducing factor on the Raman peak intensities obtained by the 20x objective.

(2) The length of the error bars is shorter for the 20x objective compared to the 50x objective. It means that there are smaller differences among the values of the Raman peak intensity that are obtained from different locations on the sample when the 20x objective is employed. In other words, the 20x objective shows better signal reproducibility than the 50x objective. Due to the round shape of the droplet, finding the exact focus is challenging. Thus, the quality of the focus is different from location to location on the sample. The accuracy of the focus affects the strength of the Raman peaks of MB. As mentioned in (1), the 20x objective is less sensitive to the exact focus point due to the lower magnification and higher effect of out-of-focus rays. Thus, the differences in Raman peak intensity from different points on the sample are less pronounced when the 20x objective is used. As a result, Raman signals are more reproducible when they are acquired using a 20x objective.

(3) The LOD and LOQ were calculated using the method described in section 3.3.4 and using equation 3.4 and 3.5, respectively. The values calculated for LOD and LOQ of MB are 2.88% and 9.62% using the 50x objective and 1.74% and 5.82% using the 20x objective.

As mentioned in (1), the 20x objective provides optimum conditions in which stronger Raman band intensities are acquired for each specific MB concentration. As a result, the Raman peaks obtained using the 20x objective are easier detectable in the solutions with lower concentrations compared to the 50x objective. Therefore, the LOD of MB is lower when the 20x objective is used.

From the experiments done in this section, it can be concluded that one of the most



FIGURE 4.10: (a) Aluminium structure designed as sample holder, (b) MB solution in the aluminium structure under the microscope of the Raman spectrometer.

important factors that affects the strength of Raman signals is the exact focus position within the Raman spectrometer. The magnification of the objective lens and the sampling geometry are two parameters affecting the accuracy of the focus. A higher magnification objective is very efficient in collecting a large amount of scattered light but also sensitive to focusing in a way that the sample geometry or any tiny vibrations along the optical axis can dramatically affect the focus and thus, the signal strength. In contrast, lower magnification objective is less sensitive to the focusing conditions and measurements done by such objective lens are therefore more reproducible.

4.4.2 Modifying sample parameter

Results obtained from MB droplet samples in section 4.4.1 show that the following modifications need to be done to improve the quality of our measurements:

- (1) For easier and more reproducible focusing, the curvature shape of the sample surface should be decreased and a flatter surface should be provided.
- (2) To achieve a more stable focus, vibrations of MB solution samples should be reduced.
- (3) To enhance the accuracy in quantifying, interpreting, and comparing the results, a more reproducible sampling method should be applied.

Dropping MB solutions on a silicon wafer is not a fully reproducible sampling method. In fact, the drops on the substrate might have different curvatures and surface areas due to the possibility of slight differences in the height and angle from which they are dropped and the different amounts of MB solution contained in individual drops.

With that in mind, we designed an aluminium structure shown in Fig. 4.10(a) as sample holder. Each hole of this structure has a radius of 0.5 cm and a depth of 0.5 cm. The

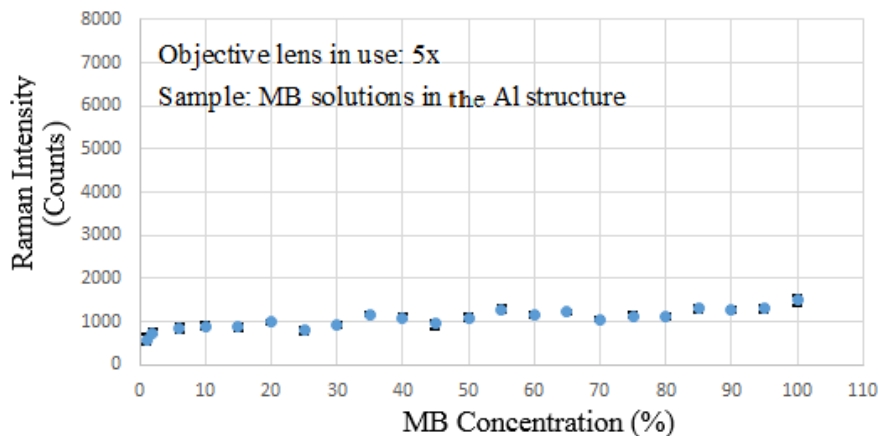


FIGURE 4.11: The intensity of the MB Raman peak at 1625 cm^{-1} vs. MB concentration obtained using the 5x objective lens from MB solutions in the aluminium structure (Excitation wavelength: 532 nm, Power at sample: 1.75 mW, Exposure time: 10s).

surface of MB solution is almost flat when each hole is filled with a suitable amount of MB solution. Moreover, this structure partially reduces the free vibrations of the solution since the solution is surrounded and restricted by it. Furthermore, since solutions with different concentrations have almost the same volume and shape when they are in this structure, it provides us with a more reproducible sampling method.

In section 4.4.3, we used this aluminium structure as sample holder and repeated the measurements done in the section 4.4.1. Then, we analyse the outcomes of the new experiments and compare them to the results achieved in section 4.4.1.

4.4.3 LOD of MB in aqueous solutions in the Al structure

In this experiment, the aluminium structure (Fig. 4.10(a)) was filled with MB aqueous solutions with low concentrations. Then, five spectra from different locations on each sample were collected by each objective lens. Results are shown in Figs. 4.11, 4.12, and 4.13.

Evaluation of the performance of the 5x objective lens for MB solutions in the Al structure

As Fig. 4.11 shows, when Raman spectra are acquired using the 5x objective from MB solutions in the aluminium structure, no specific trend between the average Raman peak intensity at 1625 cm^{-1} and the MB concentration can be observed. This implies that the 5x objective lens can be used for detecting MB, but it does not have sufficient sensitivity to identify MB concentration. Therefore, the 5x objective lens is not a proper objective to be applied for quantitative analysis, LOD, and LOQ studies. This is in agreement with the

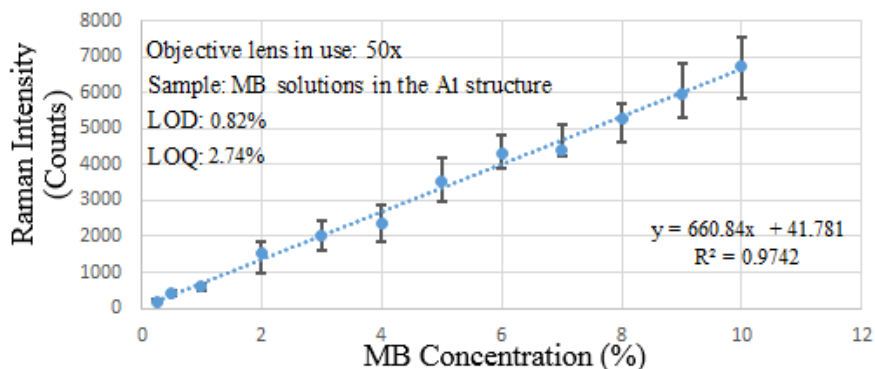


FIGURE 4.12: Intensity of the MB Raman peak at 1625 cm^{-1} vs. MB concentration obtained using the 50x objective lens from MB solutions in the aluminium structure (Excitation wavelength: 532 nm, Power at sample: 1.75 mW, Exposure time: 10s).

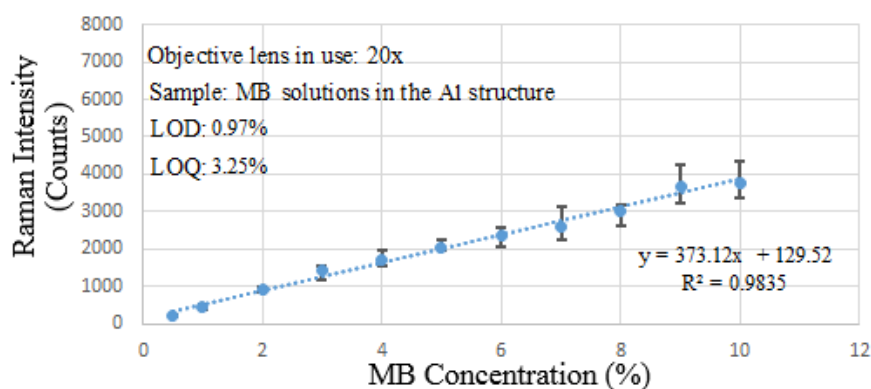


FIGURE 4.13: Intensity of the MB Raman peak at 1625 cm^{-1} vs. MB concentration obtained using the 20x objective lens from MB solutions in the aluminium structure (Excitation wavelength: 532 nm, Power at sample: 1.75 mW, Exposure time: 10s).

previous results achieved from MB droplet samples in section 4.4.1.

Evaluation of the performance of 50x and 20x objectives for MB solutions in the Al structure

A linear relationship between the average Raman peak intensity at 1625 cm^{-1} and the MB concentration is observed in Figs. 4.12 and 4.13. This linear trend agrees well with equation 2.2 and is confirmed by the values of R^2 which are close to one. Therefore, the 50x and 20x objective lenses have proper sensitivity to be used for quantitative measurements and estimating the LOD and LOQ of MB in solutions in the aluminium structure.

A comparison between Figs. 4.12 and 4.13 shows that similar to the droplet samples, the length of the error bars are shorter when Raman spectra are acquired using the 20x objective. This is due to the lower magnification of the 20x objective, which makes it less sensitive to the factors disturbing the focus.

Comparing Fig. 4.12 with Fig. 4.7 and Fig. 4.13 with Fig. 4.8 shows:

(1) The average peak intensities obtained from the samples in the aluminium structure are stronger than their counterparts acquired from MB droplets. The major reasons for the stronger signals obtained from the samples in the aluminium structure are: the bigger sample volume contributing to the signal, the better focus of the laser due to the almost flat surface of the MB solution, and less vibration or free movement of the sample owing to its restriction in the aluminium structure.

It is worth noting that the mean values of Raman peak intensities obtained from MB droplets under relatively poor conditions (small sample volume, free movement of sample, and less accurate focusing) still show a very good agreement with the linear function predicted by equation 2.2. This shows that a much smaller sample volume is enough to obtain a sufficiently high signal strength.

(2) The length of error bars or variations among measurements performed by each objective lens are lower for MB samples in the aluminium structure compared to MB droplet samples. This is due to the more stable and more reproducible focusing conditions provided by restriction of the sample and its flatter surface within the aluminium structure.

(3) The slopes of the calibration curves obtained from MB samples in the aluminium structure are higher than those acquired from MB droplets. This implies that the rate of the change of the peak intensity with respect to the MB concentration is increased by using the aluminium structure as sample holder. We believe that this is due to providing more reproducible experimental conditions using the aluminium structure. Thus, the sensitivity of the measurement system to the changes in MB concentration improves. In the case of MB droplet samples, the focus position may vary from point to point on a sample or the shape of each droplet may be different from sample to sample. Therefore, the sensitivity of the measurement system is lower for MB droplets compared to the MB solutions in the aluminium structure.

(4) When MB samples are placed in the aluminium structure, stronger average peak intensity in each concentration is obtained using the 50x objective. This is different from what we previously observed for MB droplet samples, where stronger signals were recorded using the 20x objective. The higher magnification objective, 50x, has a higher efficiency in collecting scattered signals, but is also more sensitive to the focus conditions compared to the 20x objective. As mentioned in section 4.4.1, in the case of droplets, the exact position of the laser focus on the samples was less well-defined and thus, the efficiency of the 50x objective was decreased more compared to the 20x objective. Hence, stronger signals were obtained using the 20x objective. However, when using the aluminium structure, the quality of the focus

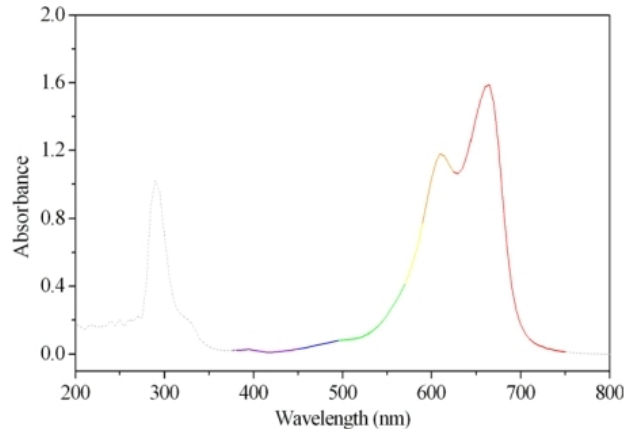


FIGURE 4.14: UV-Vis absorption spectrum of MB aqueous solution [78].

is improved in terms of stability and reproducibility due to the reasons mentioned above. Therefore, we can fully utilise the higher collection efficiency of the higher magnification objective, 50x.

It is interesting to investigate the performance of the 50x and 20x objectives for the samples in the aluminium structure in more detail. According to equation 4.3, the focal volume of a 20x objective is bigger than that of a 50x objective. However, the effective sample volume also depends on the optical properties of the sample itself. One of the important optical properties of a material that has to be considered is self-absorption. Absorption of the laser light by the sample attenuates both, the incident laser light reaching a certain volume within the sample, and the Raman shifted photons escaping that volume. The decrease in the light intensity is given by [77]:

$$I(z) = I(z = 0)e^{-\alpha z} \quad (4.5)$$

where $z = 0$ refers to the surface of the sample, z is the longitudinal sampling depth, and α is the attenuation coefficient. As Fig. 4.14 shows [78], MB aqueous solutions have a small amount of self-absorption at the 532 nm excitation wavelength. According to Table 4.1, equation 4.2, and equation 4.3, the 50x objective has a bigger collection cone but a smaller sampling depth and focal volume compared to the 20x objective. Therefore, As equation 4.5 suggests, using the 50x objective causes less attenuation of the incident laser light and the Raman-shifted light due to its lower sampling depth and higher power density at the surface of the sample compared to the 20x objective. The bigger collection cone of the 50x compared to the 20x objective also enhances the strength of Raman signals collected by the 50x objective. However, the smaller number of MB molecules in the smaller focal volume of the 50x objective reduces the strength of the Raman signal. From our experiments one can see that in each concentration, a stronger average peak intensity is obtained using the

50x objective. Therefore, the effects of enhancing factors, which are lower attenuation of light and a larger collection cone, are higher than the effect of the reducing factor, which is the lower number of MB molecules in the focal volume of the sample for the 50x objective. Hence, stronger signals can be recorded using the 50x objective compared with the 20x.

Therefore, due to the more accurate focusing of the laser light for the samples in the aluminium structure, the efficiency of the 50x objective lens is improved. However, in the case of droplets, owing to less stable and less reproducible focusing conditions, the efficiency of this objective lens decreased dramatically.

(5) The LOD and LOQ of MB samples in the aluminium structure were calculated using equations 3.4 and 3.5, respectively. The LOD and LOQ values are 0.82% and 2.74% when the 50x objective is used, and 0.97% and 3.25% when the 20x objective is used.

Compared to MB droplet samples, the LOD and the LOQ of MB decrease by 2.06% (56 μM) and 6.88% (186 μM) when the 50x objective is used and 0.77% (21 μM) and 2.57% (69 μM) when the 20x objective is applied. In fact, due to the reasons mentioned above, the stronger signal strengths obtained from MB solutions contained in the aluminium structure make MB molecules detectable even in stronger diluted solutions.

(6) The minimum LOD for the MB samples in the aluminium structure is achieved when the 50x objective lens is used. In fact, as mentioned above, stronger signals are obtained for each different concentration using the 50x objective lens, which make the MB characteristic peaks detectable in the stronger diluted solutions.

Summarising all the above observations, changing sample configuration by using an aluminium structure as sample holder leads to better focusing of the excitation laser. Therefore, we can fully exploit the advantages of the 50x objective lens to collect stronger signals in order to achieve lower LOD and LOQ for MB. However, one also has to consider that the measurements done by employing the 20x objective lens are still more reproducible compared to 50x objective lens.

4.5 Establishing analytical models and calculation of the errors

In this study, the calibration curves obtained using the 20x and 50x objective lenses are utilised to predict unknown concentrations of MB in the aqueous solutions. In fact, each calibration curve provides a linear equation that relates the average signal peak intensity to

the MB concentration. Therefore, an unknown concentration can be estimated by measuring the mean value of the peak intensity at 1625 cm^{-1} , obtained by the Raman spectrometer, and inserting it into the calibration curve equation.

However, when using the calibration curves for the prediction of an unknown concentration, one should also know how reliable a measured intensity relates to the concentration of the analyte. Therefore, in order to assess the accuracy of the calibration curves and analytical models in predicting unknown concentrations, calculating the error of estimation is important. For that, we calculated the error of prediction for MB droplet samples and MB solutions in the aluminium structure according to the following steps:

(1) We prepared standard aqueous solutions of MB (solutions with known concentrations) ranging from 100% down to 10% in steps of 5% by the method explained in section 3.3.1.

It is important to note that analytical models should be established for concentrations equal to or higher than LOQ. This is because LOQ is the lowest concentration at or above which there is confidence that the reported measurement truly reflects the actual value [80]. As calculated in sections 4.4.1 and 4.4.3, whether our samples were in droplet form or in the aluminium structure, the LOQ of MB was below 10%. Thus, we constructed our analytical models for MB concentrations equal to or higher than 10%.

(2) We put aside four out of the total numbers of the solutions made in step (1). Solutions put aside were named "*testing solutions*". In order to have testing solutions in all concentration ranges, we classified our solutions in five groups, each of which contained five solutions. That is, the first group contained 10%, 15%, 20%, 25%, and 30% solutions and the second group contained 35%, 40%, 45%, and 50% solutions and so on. We labelled the five solutions in each group from one to five, respectively. Then, we used a uniform random generator developed in MATLAB to randomly choose a number from one to five. The random generator gave us the number "two" and thus, we put aside the second solution of each group as our testing solution. Thus, our testing solutions were 15%, 40%, 65%, and 90% solutions.

(3) We obtained Raman spectra of five different locations on each standard solution made in step (1).

(4) New calibration curves in which the testing solutions and their related peak intensities were excluded were constructed by finding the line-of-best-fit through the experimental data for the remaining data points.

(5) The new calibration curves (analytical models) obtained in step (4) were used to estimate the concentration of the testing solutions. The concentrations of the testing solutions

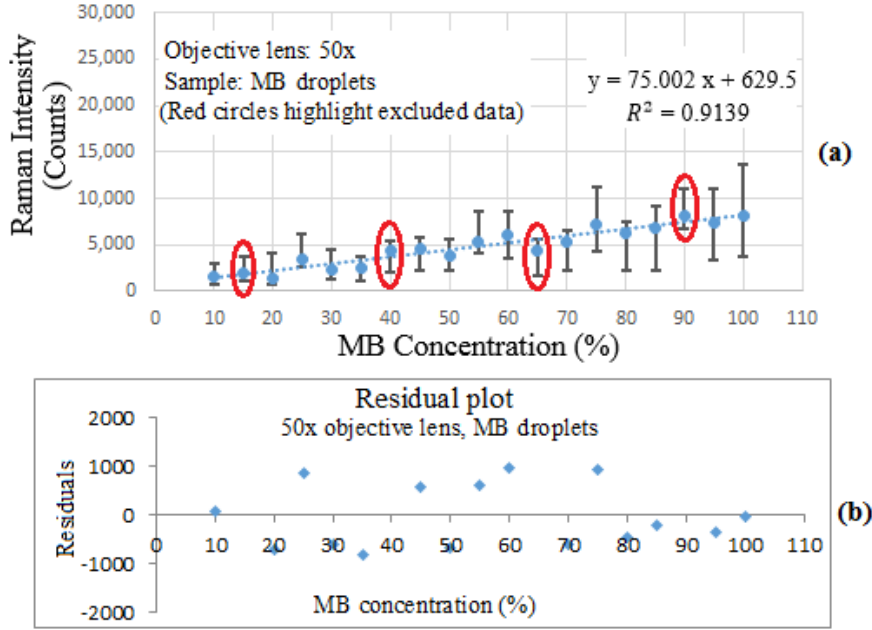


FIGURE 4.15: (a) The intensity of the MB Raman peak at 1625 cm^{-1} vs. MB concentration obtained using the 50x objective lens from MB droplets (Power at sample: 1.75 mW, Exposure time: 10s). *data marked with red circles is not used for constructing the calibration curve* (b) Residual values of the calibration curve obtained using the 50x objective lens from MB droplets.

Testing solution concentration (%)	Mean Raman intensity (Counts)	Predicted Concentration (%)	Error (%)
15	2000	18.27	21.81
40	4300	48.93	22.34
65	4461	51.08	21.4
90	8050	98.93	9.93
Average Error:			18.87

TABLE 4.2: Error estimation of the analytical model (calibration curve) predicting MB concentration in droplet samples using the 50x objective lens. Calibration curve equation: $y=75.002x+629.5$

estimated by the calibration curves are called "*predicted concentrations*".

(6) MB predicted concentrations obtained in step (5) were compared to the actual concentrations for error calculation. The error is defined as the difference between the actual concentration and the predicted concentration.

It is typical to express the error as a percentage, so the error in a testing solution was calculated using the following equation [79]:

$$Error = \frac{actual\ concentration - predicted\ concentration}{actual\ concentration} \times 100 \quad (4.6)$$

(7) The total error of the analytical model was calculated by averaging over the error in the four testing solutions.

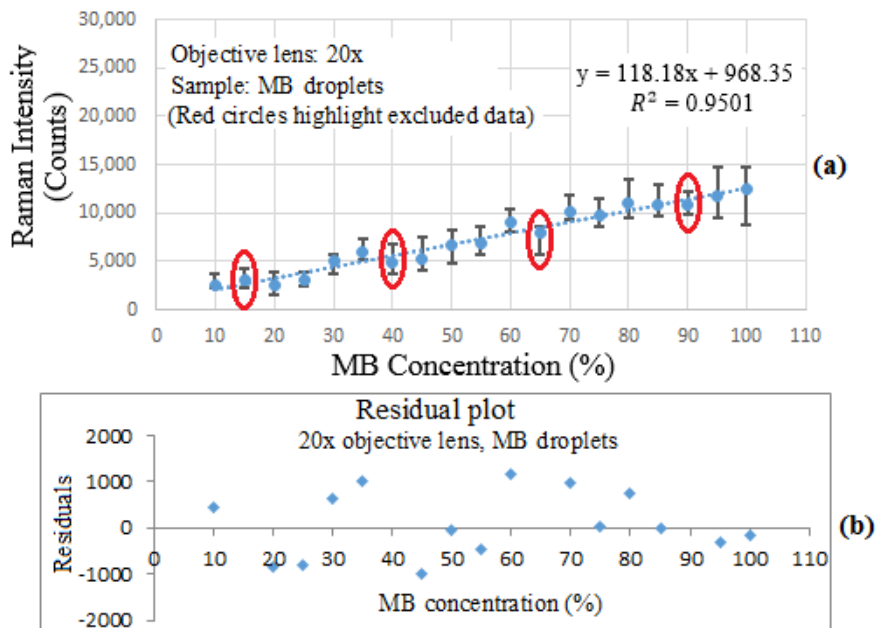


FIGURE 4.16: (a) The intensity of the MB Raman peak at 1625 cm^{-1} vs. MB concentration obtained using the 20x objective lens from MB droplets (Power at sample: 1.75 mW, Exposure time: 10s). *data marked with red circles is not used for constructing the calibration curve* (b) Residual values of the calibration curve obtained using the 20x objective lens from MB droplets.

Testing solution concentration (%)	Mean Raman intensity (Counts)	Predicted Concentration (%)	Error (%)
15	3121	18.21	21.24
40	4913	33.37	16.55
65	7921	58.83	9.49
90	10900	84.03	6.62
Average Error:			13.52

TABLE 4.3: Error estimation of the analytical model (calibration curve) predicting MB concentration in droplet samples using the 20x objective lens. Calibration curve equation: $y=118.18x+968.35$

Analytical models and error calculation for MB droplet samples

As explained above, we established new calibration curves and calculated the error of prediction for MB droplet samples. The new calibration curves and their related residual plots are shown in Fig. 4.15(a), (b) using the 50x objective and in Fig. 4.16(a), (b) using the 20x objective. As shown in Figs. 4.15(b) and 4.16(b), residuals behave randomly indicating that the models fit the experimental data well. If the residuals displayed a systematic pattern, it would be a sign that the models fit the data only poorly.

Tables 4.2 and 4.3 show the error in each testing solution and the total error of prediction of the analytical models when the 50x and the 20x objective lenses are applied. A set of Raman spectra collected using the 50x and the 20x objective lenses from MB droplets with different concentrations is shown in Figs. A.5 and A.6 in the appendix.

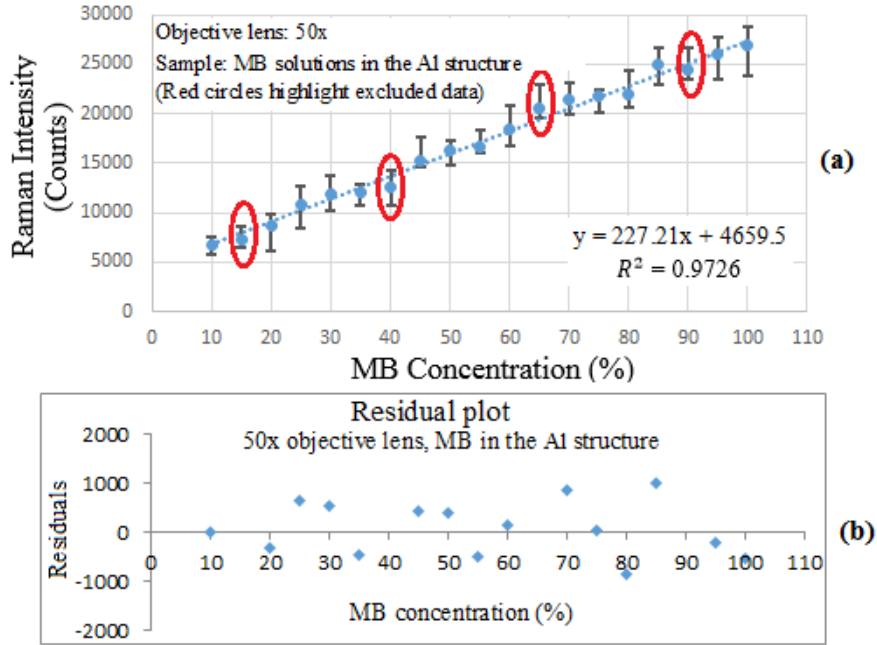


FIGURE 4.17: (a) The intensity of the MB Raman peak at 1625 cm^{-1} vs. MB concentration obtained using the 50x objective lens from MB solutions in the Al structure (Power at sample: 1.75 mW, Exposure time: 10s). *data marked with red circles is not used for constructing the calibration curve* (b) Residual values of the calibration curve obtained using the 50x objective lens from MB solutions in the Al structure.

Testing solution concentration (%)	Mean Raman intensity (Counts)	Predicted Concentration (%)	Error (%)
15	7350	11.84	21.05
40	12659	35.20	11.98
65	20564	69.99	7.69
90	24360	86.70	3.65
Average Error:			11.09

TABLE 4.4: Error estimation of the analytical model (calibration curve) predicting the concentration of MB aqueous solutions in the Al structure using the 50x objective lens. Calibration curve equation: $y=227.2x+4659.5$

Analytical models and error calculation for MB solutions in the Al structure

New calibration curves and the error of prediction of the analytical models for MB solutions in the aluminium structure were obtained by employing the same method described above. Calibration curves and their corresponding residual plots are shown in Fig. 4.17(a), (b) and Fig. 4.18(a), (b) using the 50x and 20x objective lenses respectively. Since no systematic pattern can be seen in Figs. 4.17(b) and 4.18(b), and since the variations of the residuals are random, we can conclude that the models fit the experimental data strongly.

Error in each testing solution and the total error of prediction using the 50x and the 20x objectives have been calculated and are shown in Tables 4.4 and 4.5, respectively. A set of Raman spectra collected using the 50x and the 20x objectives from MB solutions in the

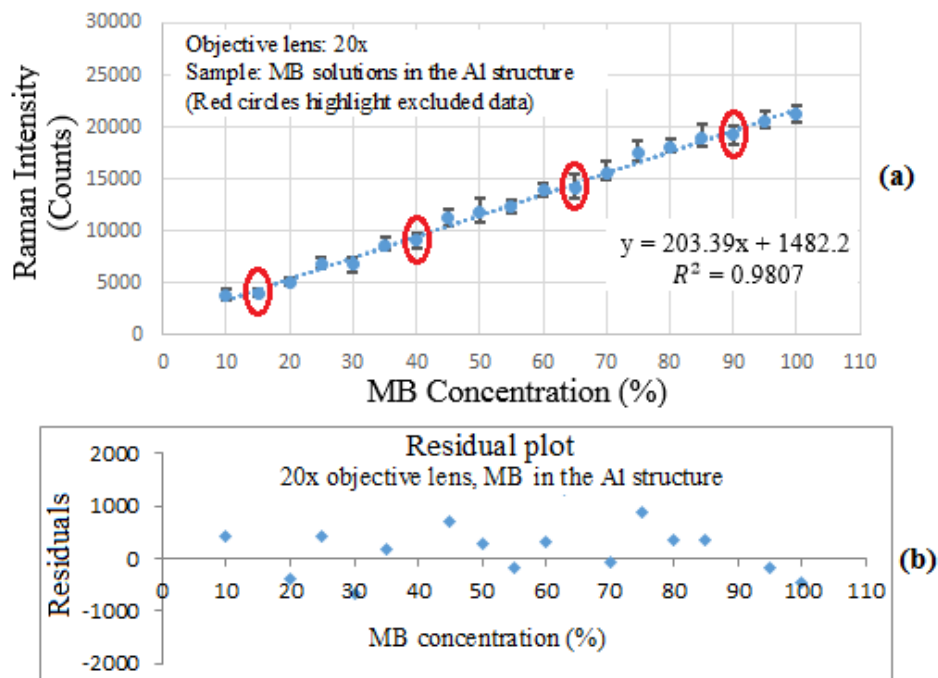


FIGURE 4.18: (a) The intensity of the MB Raman peak at 1625 cm^{-1} vs. MB concentration obtained using the 20x objective lens from MB solutions in the Al structure (Power at sample: 1.75 mW, Exposure time: 10s). *data marked with red circles is not used for constructing the calibration curve*(b) Residual values of the calibration curve obtained using the 20x objective lens from MB solutions in the Al structure.

Testing solution concentration (%)	Mean Raman intensity (Counts)	Predicted Concentration (%)	Error (%)
15	3900	11.88	20.74
40	9028	37.1	7.24
65	14068	61.88	4.79
90	19200	87.11	3.20
Average Error:			9

TABLE 4.5: Error estimation of the analytical model (calibration curve) predicting the concentration of MB aqueous solutions in the Al structure using the 20x objective lens. Calibration curve equation: $y=203.39x+1482.2$

aluminium structure with varying concentrations is also shown in Figs. A.7 and A.8 in the appendix.

4.6 Comparison of the results of the quantitative analysis of MB in different sample configurations

Table 4.6 shows a summary of the LOD, LOQ, and the error of the analytical models obtained using the 50x and 20x objectives. As shown in this Table, the lowest LOD and LOQ of MB are obtained when using the 50x objective lens and MB solutions in the aluminium structure.

Objective lens	Sample	LOD	LOQ	Error (%)
50x	MB Droplets	2.88%= 78 μM	9.62%=260 μM	18.87
50x	MB solutions in the Al structure	0.82%=22 μM	2.74%=74 μM	11.9
20x	MB Droplets	1.74%=47 μM	5.82%=157 μM	13.52
20x	MB solutions in the Al structure	0.97%=26 μM	3.25%=88 μM	9

TABLE 4.6: Summary of the quantitative analysis of MB droplets and MB solutions in the Al structure.

Objective lens	LOD reduction	LOQ reduction	Error reduction (%)
50x	2.06% = 56 μM	6.88% = 186 μM	7.78
20x	0.77% = 21 μM	2.57% = 69 μM	4.52

TABLE 4.7: Reduction in the LOD and LOQ of MB and the error of the analytical models by changing the sample configuration from MB droplets to MB solutions in the Al structure.

However, the lowest error of prediction corresponds to the analytical model that was derived using the 20x objective and MB solutions in the aluminium structure. Moreover, Table 4.7 shows a reduction in the LOD and LOQ of MB and the error of the analytical models by changing the sample configuration from MB droplet to MB solution in the aluminium structure.

The error can be caused by sample, instrument or procedural effects. Some sample errors include variations in sample alignment due to vibrations (e.g. from an illumination source or computer fan), sample heterogeneity due to a solution containing bubbles or not being mixed properly, or a curved shape of the sample surface causing challenges in finding an accurate focus position. Moreover, calibration errors, variation in the laser intensity, and variability of the detector response are some examples of the possible sources of the instrumental errors. Furthermore, procedural errors may be due to failure in finding the exact focus or keeping all the experimental conditions exactly the same when testing different samples. Detailed descriptions of the possible sources of error are provided in [43, 72].

In summary, in our experiments, the optimum sample configuration for direct measurement of MB concentration is the MB solution in the aluminium structure. If we use a 50x objective lens to collect the Raman spectra in this sample configuration, LOD and LOQ are lower, whereas the error of the analytical model are higher compared with a 20x objective. This is because the 50x objective lens is more sensitive and therefore, more vulnerable to the above-mentioned factors associated with measurement uncertainties. Thus, although stronger signals can be obtained by using a higher magnification objective, 50x, the overall reproducibility of the signals is improved by choosing a lower magnification objective, 20x.

5

Conclusions and future works

5.1 Summary and research outcomes

Raman spectroscopy is a well-documented and non-destructive optical technique with a high spectral resolution. It is based on irradiating a sample with an excitation laser and studying the spectrum of the inelastic scattered light leaving the sample. The frequency change of this scattered light corresponds to the rotational and vibrational frequency band structure of the scattering molecules. Thus, fingerprint information about specific molecules can be provided by this technique and it can provide qualitative and quantitative information about compositions of different samples. Therefore, Raman spectroscopy is a technique well-suited for chemical analysis from the rapid identification of unknown components to characterising materials in detail.

In this research work, we applied Raman spectroscopy for quantitative analysis on an analyte of practical importance, MB. We chose 532 nm and 1.75 mW as the optimum excitation wavelength and power at the sample by considering the quality of the measured Raman spectra and the damage threshold of the sample. Furthermore, a quantitative analysis on MB samples was accomplished by a uni-variate analysis and linear regression, correlating the peak height at a Raman shift of 1625 cm^{-1} (i.e. the highest Raman peak) with the

MB concentration. The MB Raman peak intensity at 1625 cm^{-1} was measured down to the minimum detectable concentration of different MB samples under different illumination and sample configurations. To reduce systematic and random errors in our measurements, a baseline correction was performed and measurements were repeated five times on each sample with a specific concentration. The LOD and LOQ of MB were calculated and experimental conditions were optimised to improve the results. Finally, analytical models were derived and their error of prediction was calculated and discussed.

Firstly, to study the performance of our Raman instrument, we used silicon as a reference sample material. We did various measurements using the 50x, 20x, and 5x objective lenses and the Raman peak intensity of the silicon peak at 520.5 cm^{-1} was plotted against the solid angle of the collection cone of the different objectives. The results showed that for an opaque (silicon is considered an opaque sample for the 532 nm excitation wavelength) and isotropic sample, the efficiency of objective lenses in collecting strong Raman signals increased as the numerical aperture increased. Therefore, the efficiency of objective lenses increases from 5x to 50x objective lenses.

Secondly, to avoid the so-called coffee-ring effect and to create a uniform distribution of positively charged MB molecules after drying on a silicon wafer, we negatively charged a silicon wafer. However, this method did not lead to the desired outcome in producing a homogeneous pattern of MB molecules and only marginally reduced the coffee-ring effect. Thus, such solid MB samples could not be used for quantitative analysis. Then, the sensitivity of different objective lenses with respect to sample inhomogeneity was investigated. We concluded that the lower the magnification of the objective lens, the less sensitive it was to the inhomogeneity. Therefore, sample inhomogeneity-related errors increase from 5x objective to 50x objective lenses.

Thirdly, to avoid problems associated with inhomogeneity, we collected Raman signals directly from MB aqueous solutions in droplet form. Plots of Raman peak intensity vs. concentration of MB droplets showed no specific trend for data collected using a 5x objective. Thus, we concluded that although this objective could be used for detecting MB, it did not have enough sensitivity to be used for a quantitative analysis. However, 50x and 20x objectives could be used for quantitative analysis due to the linear trend observed between the Raman peak intensity and the MB concentration. We applied linear regression for calculation of the LOD and LOQ of MB. LOD and LOQ were 2.88% and 9.62% using the 50x, and 1.74% and 5.82% using the 20x objective lenses, respectively. Based on our results, stronger Raman signals, lower LOD and LOQ, and higher measurement reproducibility were obtained using a 20x objective compared to a 50x objective. Thus, for MB droplet samples,

a 20x objective is better suited compared to a 50x objective lens.

Fourthly, in an attempt to provide more accurate and stable focusing conditions and a more reproducible sampling method in order to improve the quantitative results, an aluminium structure was designed as a sample holder. MB aqueous solutions with different concentrations were put into the aluminium structure and all the experiments were repeated. Similar to the results previously achieved for MB droplets, there was no specific trend between the MB peak intensity and the MB concentration when a 5x objective lens was employed. As a result, while MB molecules could be detected using a 5x objective, this objective is not sensitive enough for being applied for quantitative analysis. However, due to the linear relationship between the MB peak intensity and the MB concentration that was obtained by using the 50x and 20x objective lenses, we could use those results for quantitative analysis. The LOD and LOQ of MB were measured to be 0.82% and 2.74% when using the 50x, and 0.97% and 3.25% when using the 20x objective lenses, respectively. Compared with MB droplets, using an aluminium structure as a sample holder showed 2.06% ($56 \mu M$) and 6.88% ($186 \mu M$) reduction in the LOD and LOQ when using the 50x objective and 0.77% ($21 \mu M$) and 2.57% ($69 \mu M$) reduction in the LOD and LOQ when using the 20x objective, respectively. The overall variations in data measurement also decreased when using the aluminium structure and measurements showed better reproducibility. Moreover, in contrast with MB samples in droplet form, stronger Raman signals and lower LOD and LOQ were obtained when using a 50x objective. In fact, this sample modification allowed us to fully exploit the higher sensitivity of the 50x objective lens. Hence, for MB aqueous solution in the aluminium structure, the efficiency of the 50x objective was higher compared to the 20x objective. However, better measurement reproducibility was still observed when using the 20x objective.

Finally, analytical models for MB droplets and MB aqueous solutions in the aluminium structure with concentrations equal to or higher than LOQ were established and errors of prediction were calculated. For MB droplets, errors were estimated to be 18.87% and 13.52% when applying the 50x and the 20x objective lenses, respectively. For MB samples in the aluminium structure, the calculated errors were reduced to 11.9% and 9%, respectively. This means that errors were reduced by 7.78% and 4.52% for 50x and 20x objective lenses when an aluminium structure was used as sample holder. Moreover, the lowest error was obtained by an analytical model that was based on measurements with a 20x objective lens, which confirms the better reproducibility of the measurements using this objective lens.

In a nutshell, in this study, vast amount of study done among literatures provided us with a great insight into Raman spectroscopy. Moreover, systematic sequences of experiments

were done to find optimum experimental conditions under which LOD, LOQ, and the error of analytical models could be minimised. In detail, we have shown that the excitation laser wavelength and power, the accuracy of the focus, the objective lens used (excitation and collection optics), the sample configuration, and the optical properties of the sample (sample transparency) can all strongly affect the quality of Raman measurements. We demonstrated that factors related to the instrument, sample, and signal must be considered depending on the individual application and the experimental setup must be optimised to obtain best results. Moreover, we found that for opaque and lightly turbid samples higher magnification objectives result in stronger signals, but these objective lenses are also more sensitive to random errors and errors related to incomplete focusing, inhomogeneity of the sample, etc. Thus, for such samples, lower magnification objectives lead to a better reproducibility of the measurements.

5.1.1 Future works

In this study, Raman measurements were performed in laboratory conditions and our samples contained pristine molecules, MB, or MB mixed with water which is a weak Raman scatterer. Therefore, uni-variate analysis was a proper method for quantitative analysis and establishing an analytical model. However, for the on-site analysis of a variety of chemical for many applications, including sensitive detection and quantification of food contaminants (such as pesticides on different plants like fruits or crops), toxins found in the environment (such as toxic chemicals in the stream water), and so forth, we need to do remote analysis by quantitative fibre-optic Raman spectroscopy on mixture of chemical compounds. In such situations, we will have to analyse Raman spectra of samples in the presence of interfering factors. Moreover, different samples with different optical properties in a challenging environment and/or on challenging substrates with different geometries will have to be investigated.

Our future work is divided into two phases related to the direct and indirect analyses of samples using fibre-optic Raman spectroscopy: In the direct case, the optical fibre is the probe and no chemical-specific sensor element is applied. In the indirect case, some modifications are done to the fibre optic system and coatings that are sensitive to the presence of a specific chemical species are applied.

In the first phase of the future project (direct measurement), firstly, a sensitive fibre optic probe for a given sample type will be developed under consideration of the probe size, working distance, laser spot size, depth of focus, number of the collection fibres and sample

configuration. The transparency of the samples also will affect the system since, as discussed in this thesis, for opaque samples higher magnification objectives can provide stronger Raman signals, whereas as shown in Fig. A.9 in the appendix, lower magnification objectives work better for transparent samples. Then, Raman spectra of complicated analytes, containing multiple molecules will be measured. In this case, many Raman peaks overlap and have to be interpreted and the prediction of molecule concentrations has to be done in the presence of interfering factors. Thus, multivariate analysis, such as PLS and PCA, using a number of variables, has to be applied to acquire quantitative data. Besides, methods for fluorescence suppression will be investigated in order to develop a reliable automated background correction algorithm that is applicable on varying backgrounds on different spectra. In addition, experimental conditions will be optimised to decrease the LOD and LOQ and the error of our analytical models. This will be done by studying the properties of the PLS algorithm to find out how spectral noise, wavelength range selection and etc. affect the prediction uncertainty. By understanding these effects, we will be able to establish custom-designed experiments for the measurement of the concentration of specific analytes. We will develop algorithms that can produce chemical identification and quantitative measurements of concentrations of our samples. Therefore, probe sensitivity, Background discrimination, sample properties, coupling efficiency, damage threshold, and so forth will be studied.

In the second phase of the project (indirect measurement), to achieve the minimum LOD and LOQ of our probe molecules and high sensitivity and specificity, Raman signals will be enhanced by applying an optical fibre based SERS sensor. A proper nanostructured metal surface will be fabricated on the tip of an optical fibre using oblique angle deposition (OAD) technique. It is a cost effective technique with an acceptable flexibility and reproducibility that can be applied for fabrication of a SERS substrate on the tip of a fibre. The effect of morphological changes of the deposited thin metal film on the SERS response will be studied and it will be tried to achieve a high degree of sensitivity and reproducibility. After constructing a SERS optrode sensor, different optical fibres, including single mode, step-index and graded-index fibres will be tested to find the optimum practical use of the optrode sensor for detection and quantification of analytes which will be commonly-used pesticides such as Carbaryl and Dimethoate on the surface of the fruits or plants (Raman spectra of Carbaryl and Dimethoate powder are also provided in Fig. A.10 and Fig. A.11 in the appendix). As a result, an optimised Raman system that can be used for detection and quantification of tiny amounts of such pesticides on the surface of plants or fruits in remote sensing applications will be developed.



Appendix



FIGURE A.1: The photograph of our Renishaw InVia Raman spectrometer.

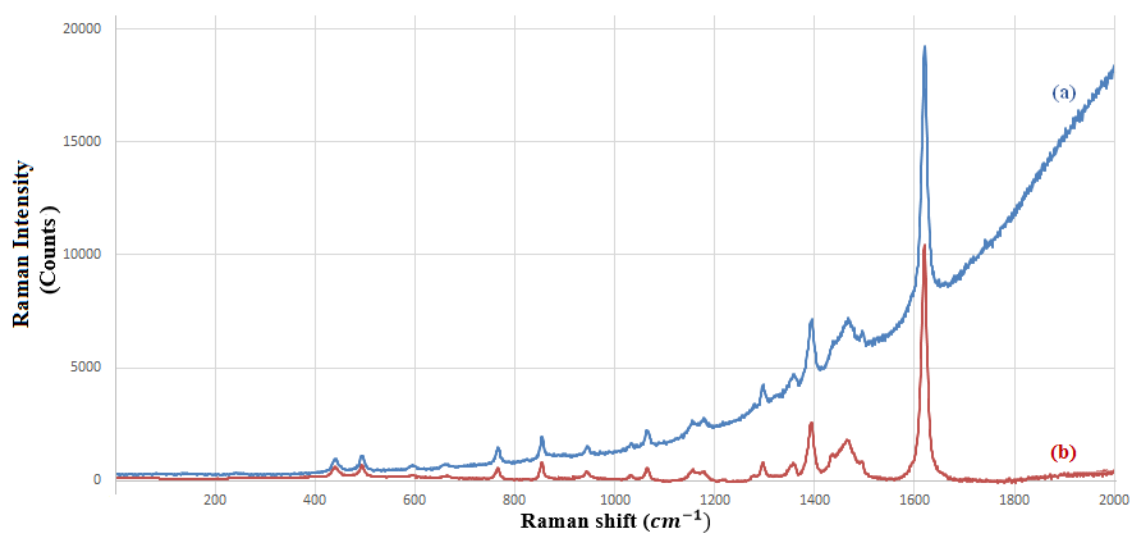


FIGURE A.2: Raman spectrum of 25% MB aqueous solution (a) before and (b) after baseline correction.

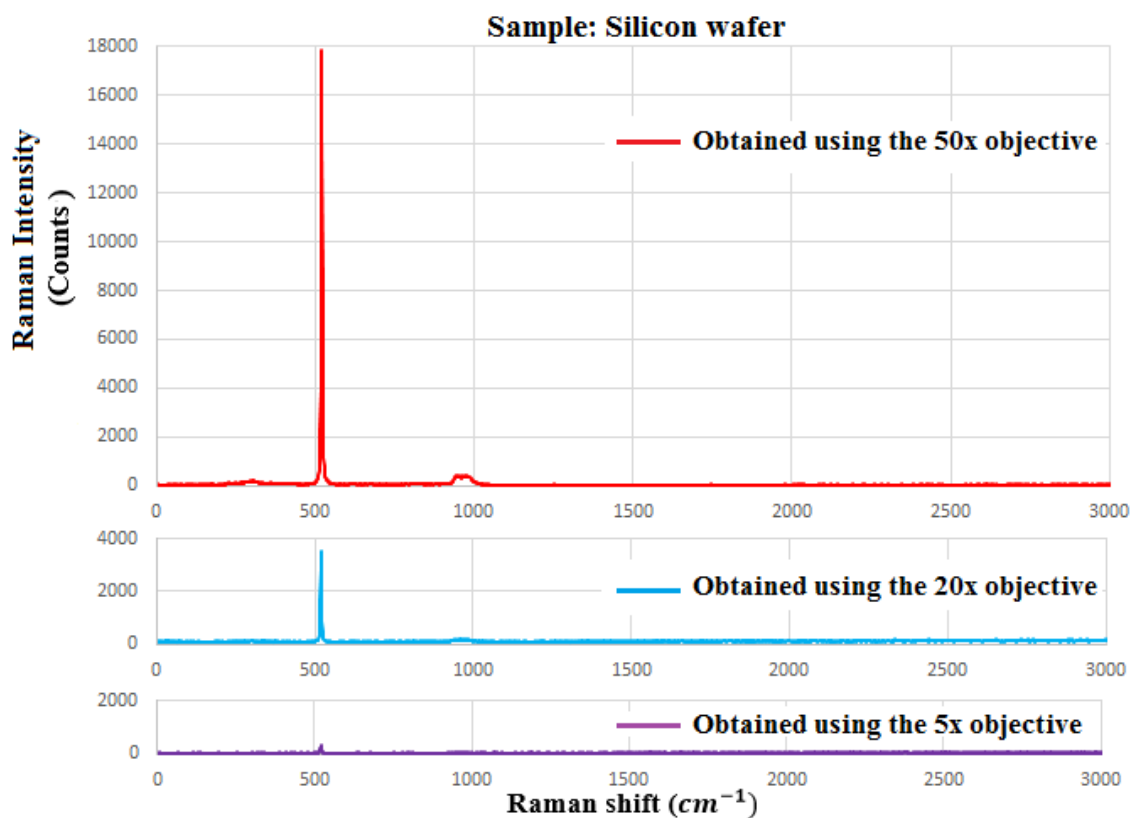


FIGURE A.3: Raman spectra of silicon wafer obtained using the 50x, 20x, and 5x objective lenses (Excitation wavelength: 532 nm, Power at sample: 1.75 mW, Exposure time: 10s).

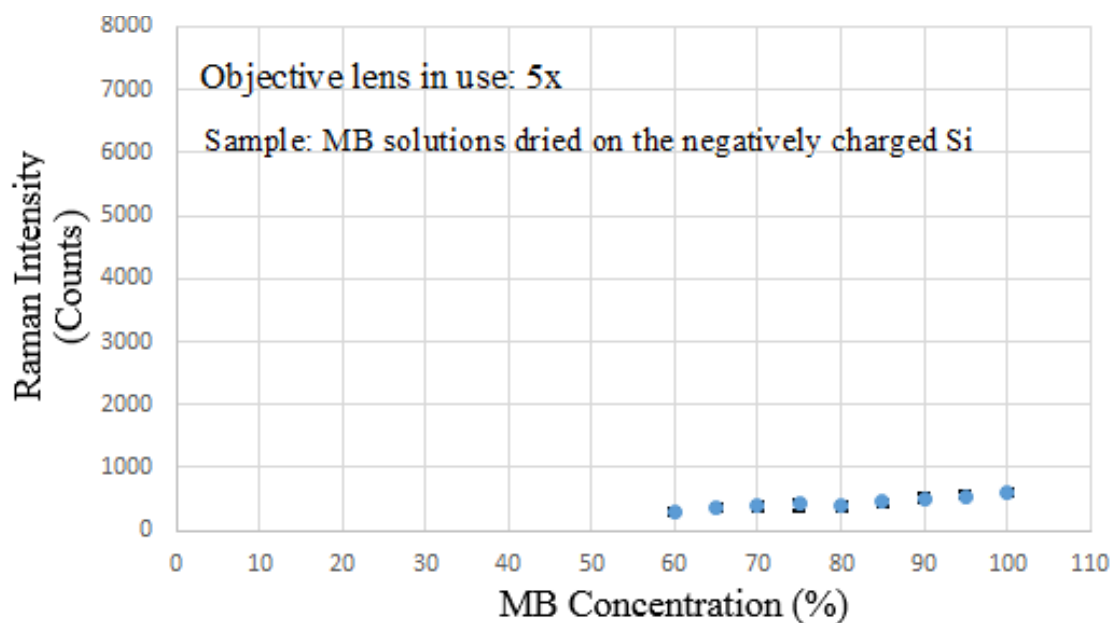


FIGURE A.4: The intensity of the MB Raman peak at 1625 cm^{-1} vs. MB concentration obtained using the 5x objective lens from MB droplets dried on the surface of negatively charged silicon (Excitation wavelength: 532 nm, Power at sample: 1.75 mW, Exposure time: 10s).

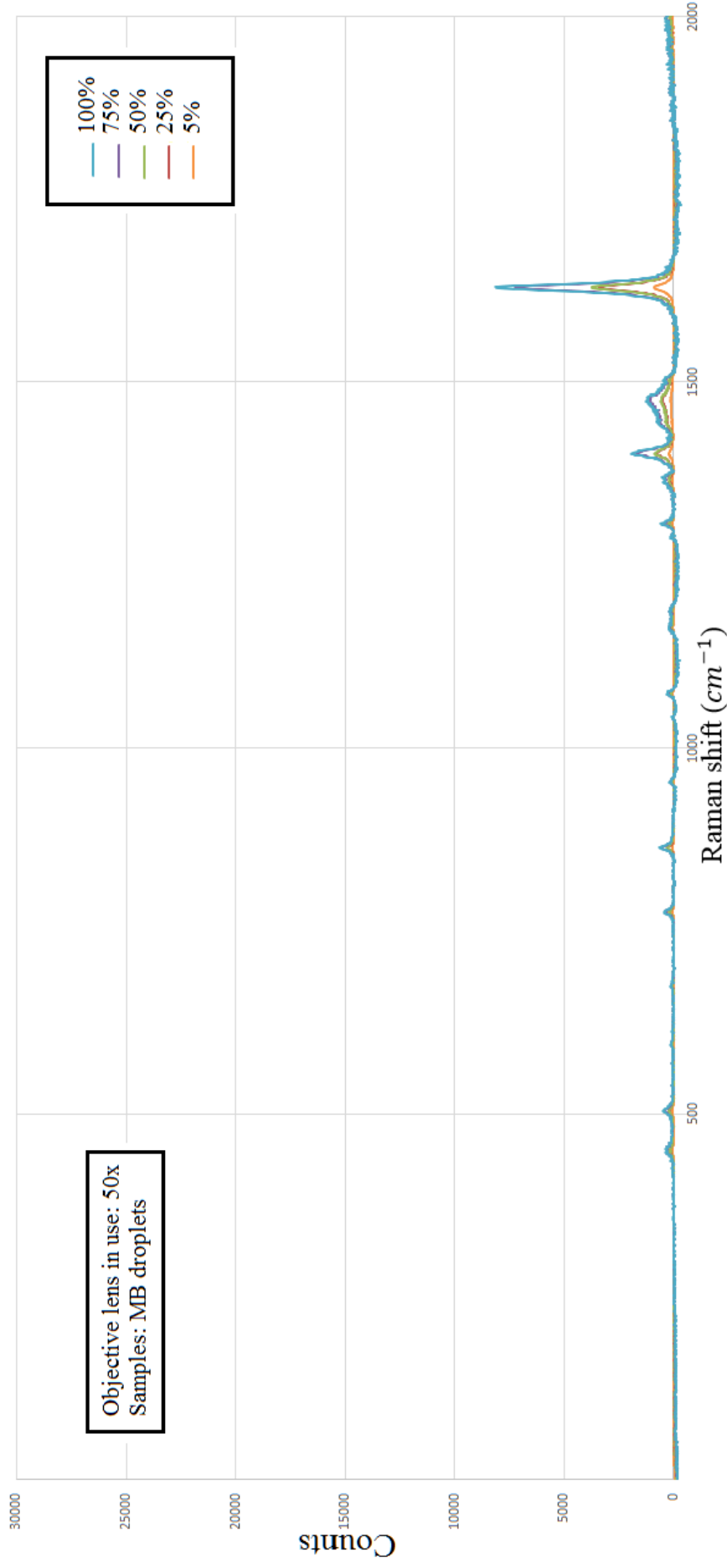


FIGURE A.5: Raman spectra of MB droplets in different concentrations after baseline correction (Only five spectra are plotted for better clarity). [Objective lens in use: 50x, Excitation wavelength: 532 nm, Power at sample: 1.75 mW, Integration time: 10s]

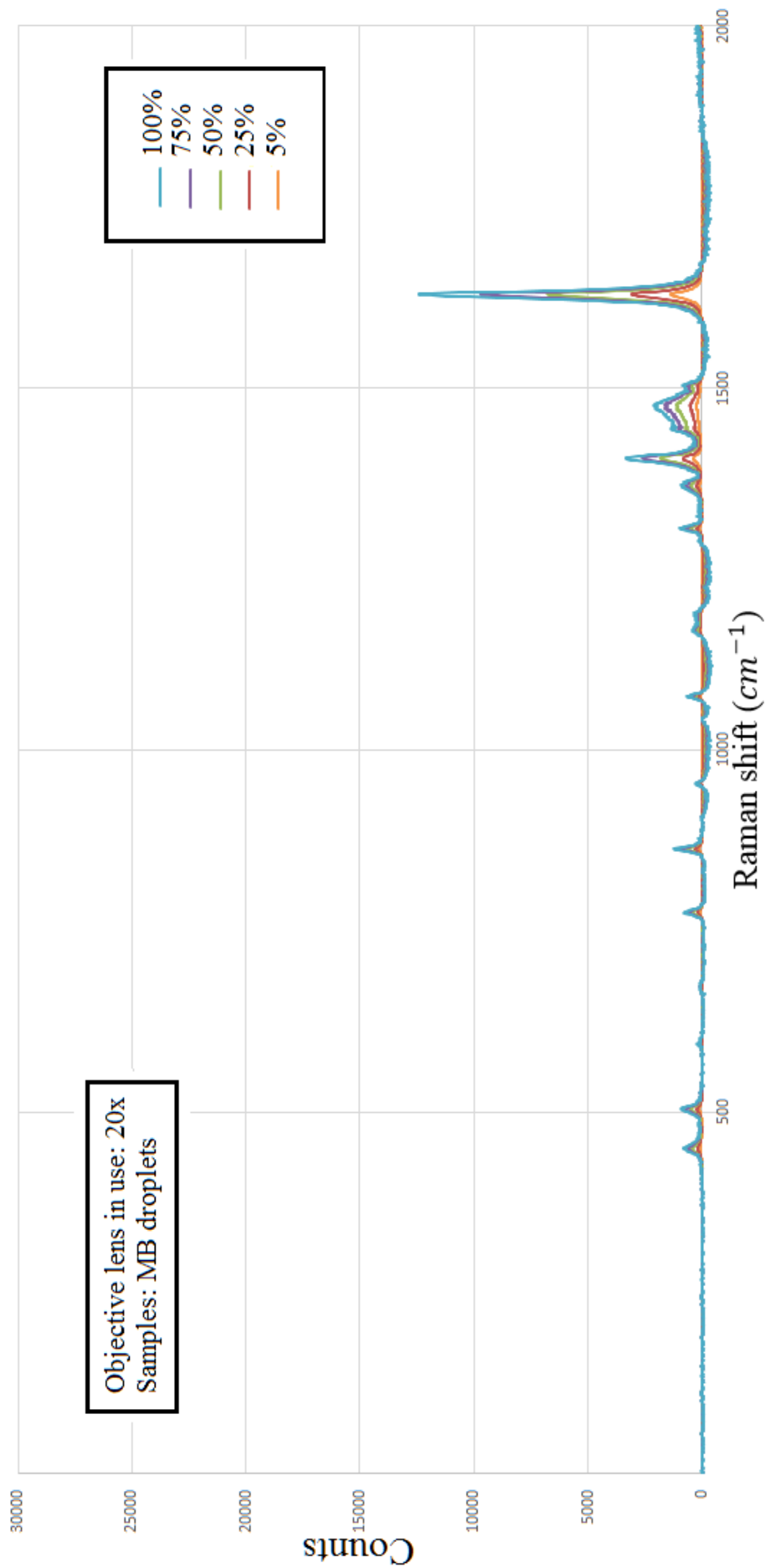


FIGURE A.6: Raman spectra of MB droplets in different concentrations after baseline correction (Only five spectra are plotted for better clarity). [Objective lens in use: 20x, Excitation wavelength: 532 nm, Power at sample: 1.75 mW, Integration time: 10s]

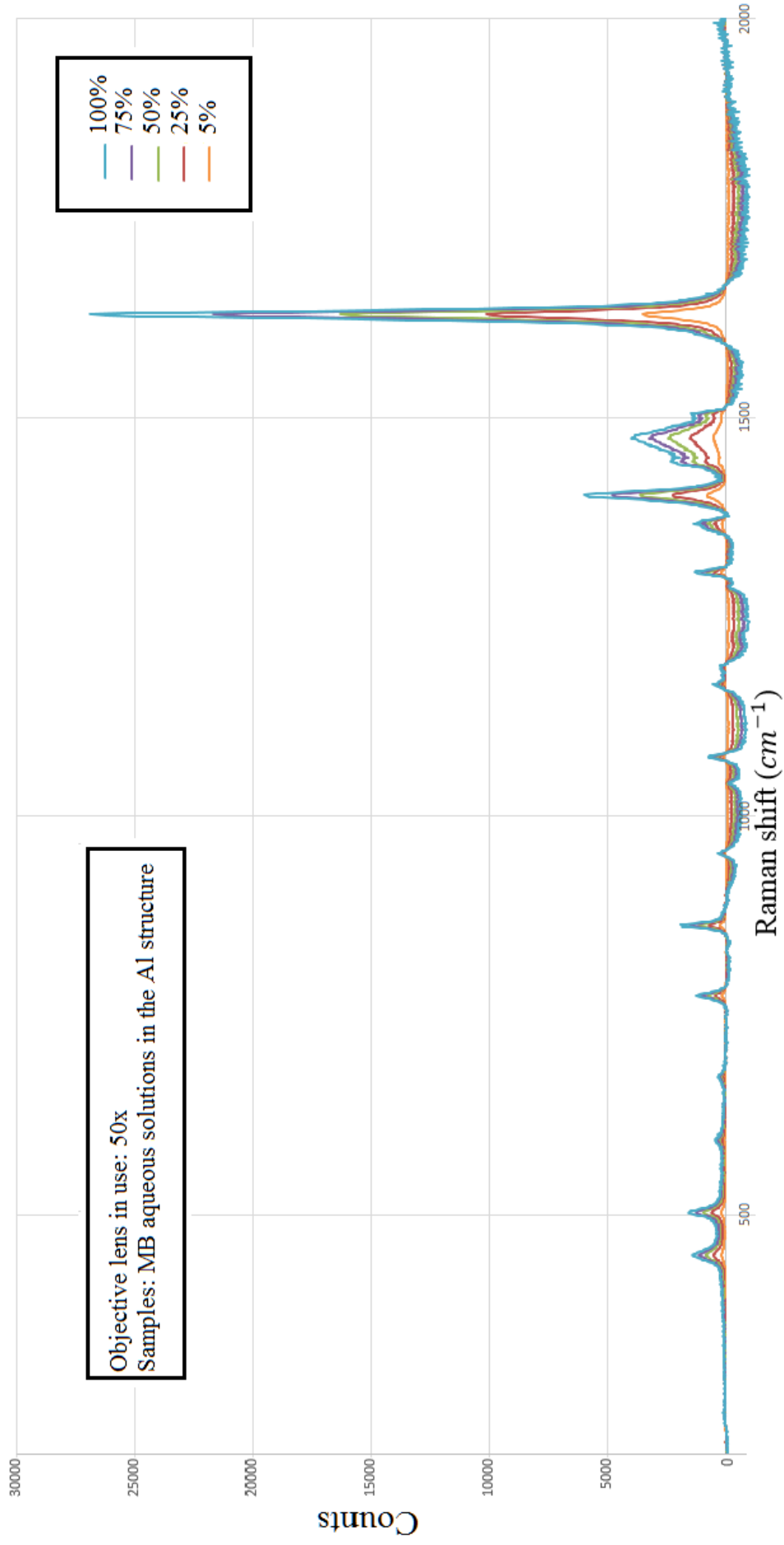


FIGURE A.7: Raman spectra of MB aqueous solutions in the aluminium structure in different concentrations after baseline correction (Only five spectra are plotted for better clarity). [Objective lens in use: 50x, Excitation wavelength: 532 nm, Power at sample: 1.75 mW, Integration time: 10s]

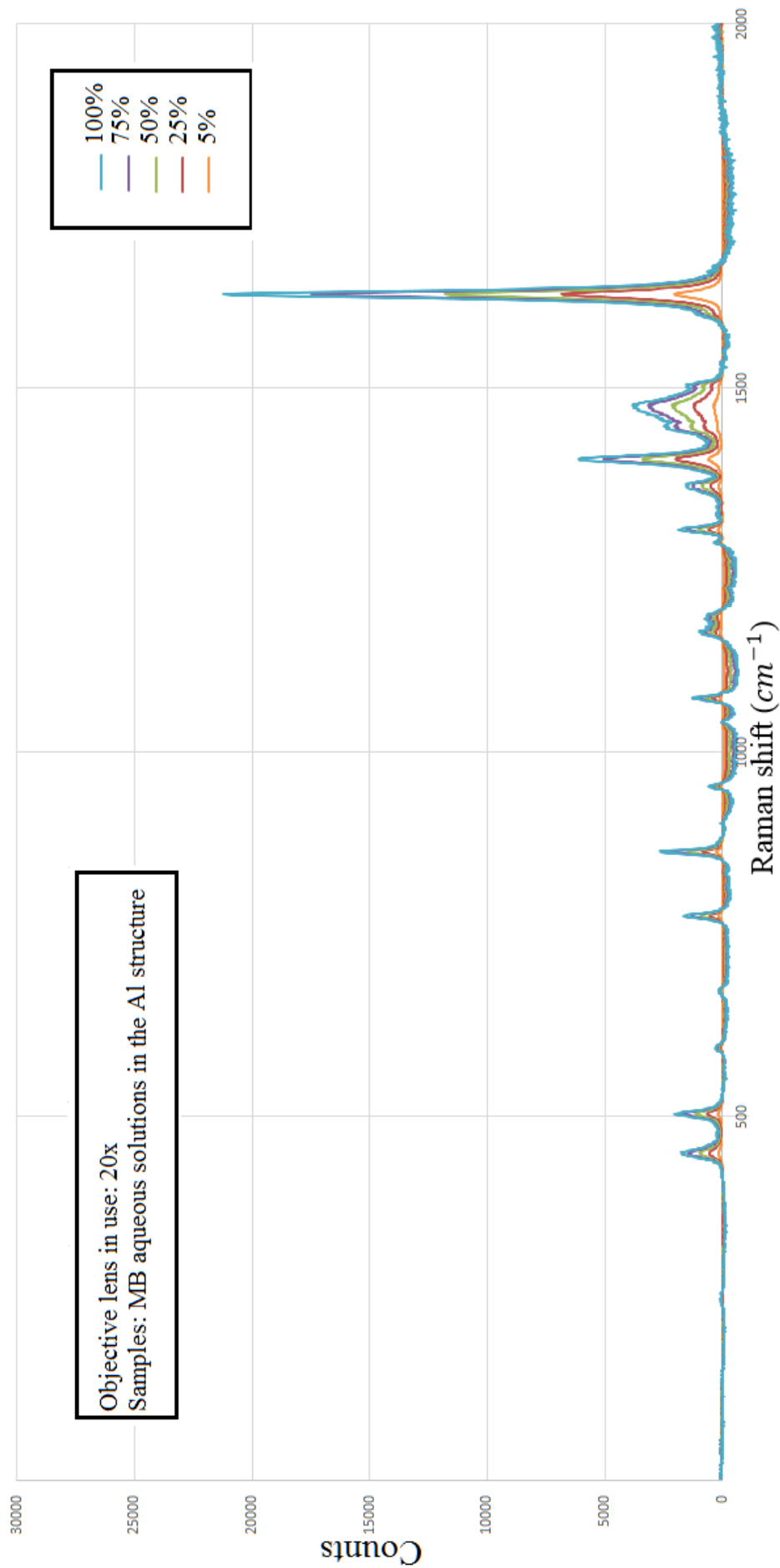


FIGURE A.8: Raman spectra of MB aqueous solutions in the aluminium structure in different concentrations after baseline correction (Only five spectra are plotted for better clarity). [Objective lens in use: 20x, Excitation wavelength: 532 nm, Power at sample: 1.75 mW, Integration time: 10s]

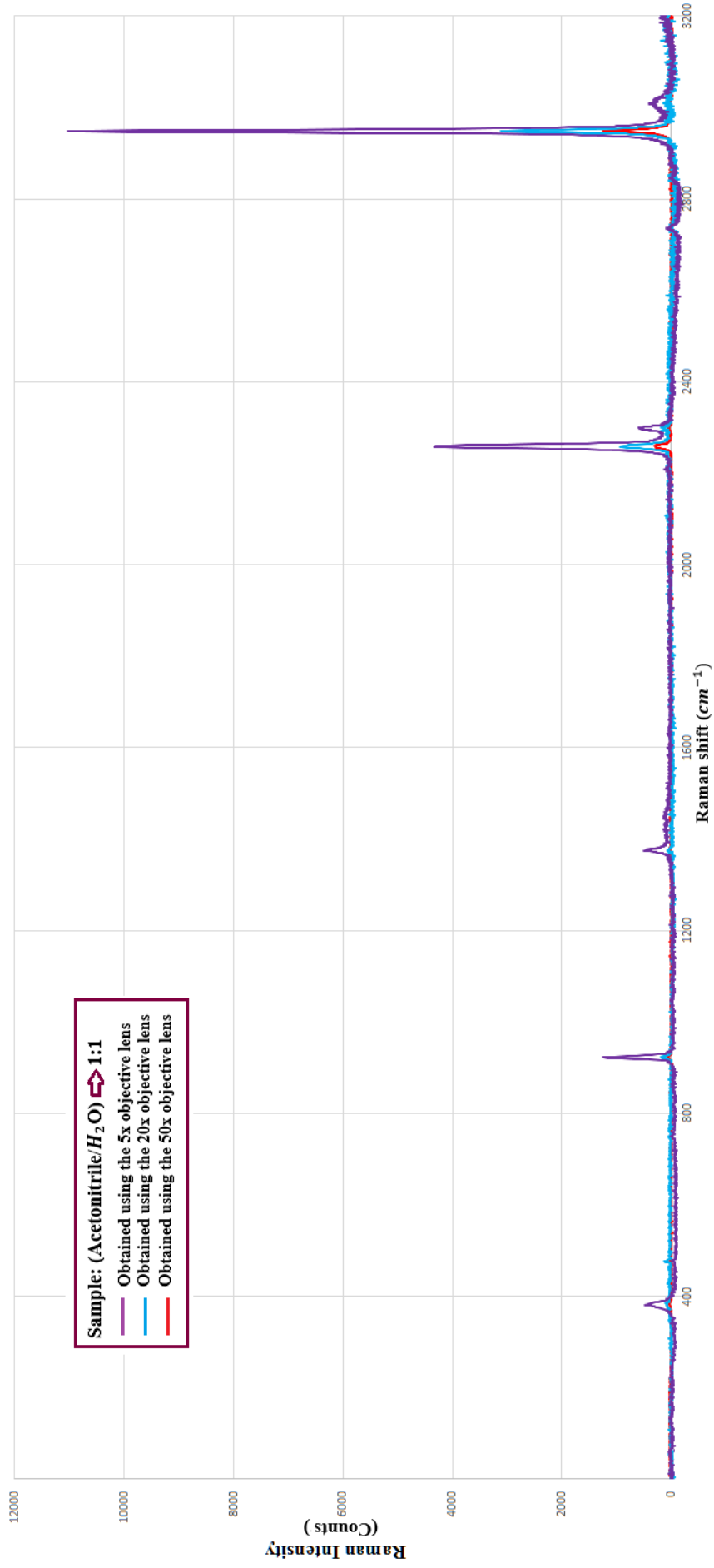


FIGURE A.9: Raman spectra of Acetonitrile/ H_2O) = 1:1 solution in the aluminium structure obtained using the 5x, 20x, and 50x objective lenses (Excitation wavelength: 532 nm, Power at sample: 1.5 mW, Exposure time: 10s, Baseline is set to zero).

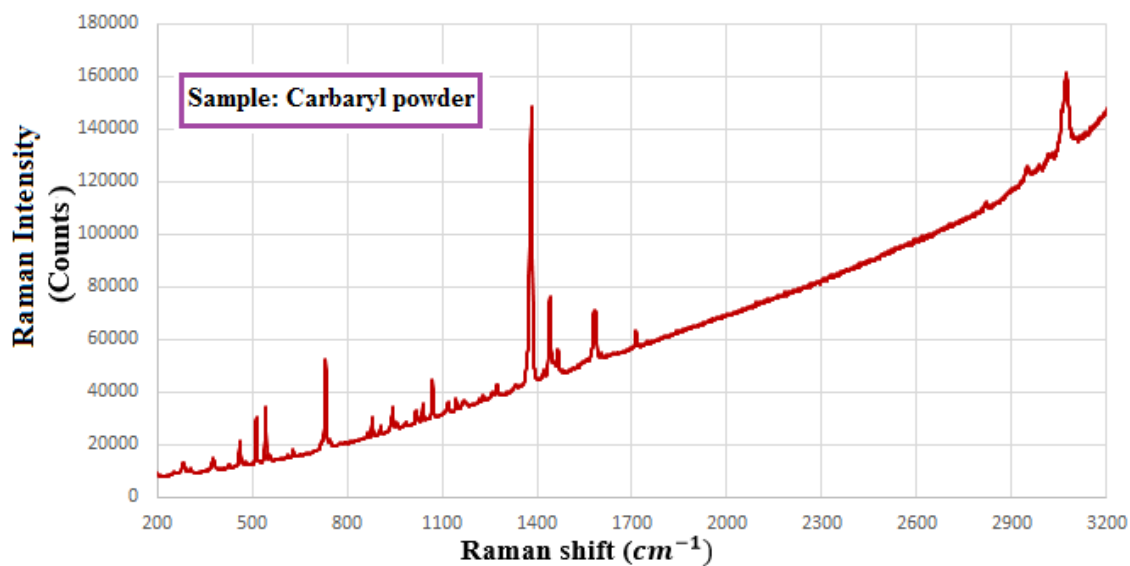


FIGURE A.10: Raman spectrum of Carbaryl powder on the silicon surface before baseline correction (Objective lens in use: 5x, Excitation wavelength: 532 nm, Power at sample: 17 mW, Exposure time: 60s).

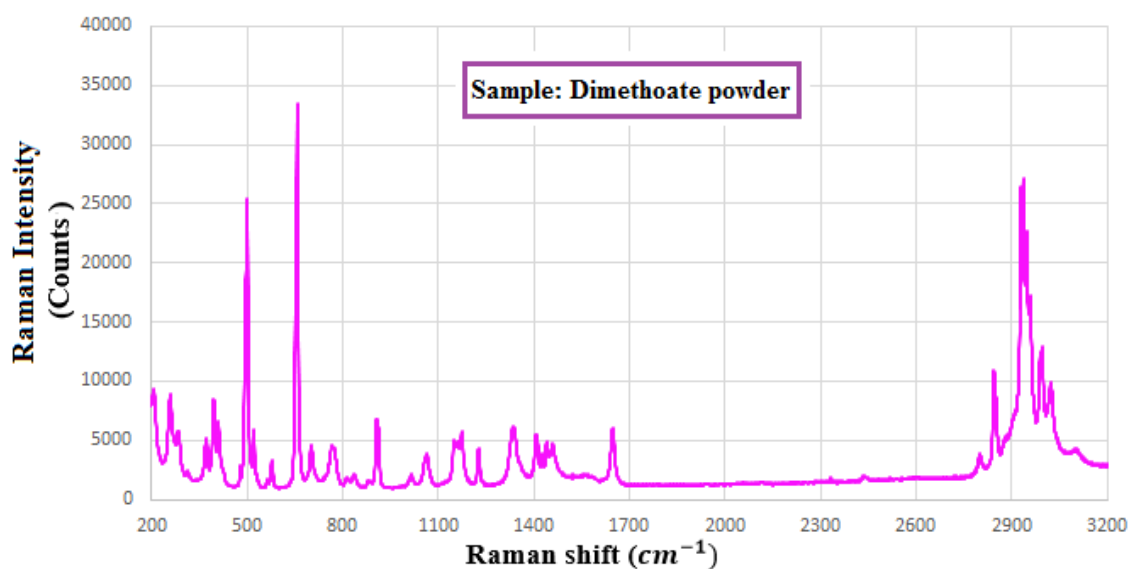


FIGURE A.11: Raman spectrum of Dimethoate powder on the silicon surface before baseline correction (Objective lens in use: 5x, Excitation wavelength: 532 nm, Power at sample: 17 mW, Exposure time: 60s).

List of Acronyms/Abbreviations

<i>CCD</i>	Charge-Coupled Device
<i>CW</i>	Continuous Wave
<i>FTIR</i>	Fourier Transform Infrared
<i>IR</i>	Infrared
<i>LOD</i>	Limit of detection
<i>LOQ</i>	Limit of Quantification
<i>MB</i>	Methylene Blue
<i>NA</i>	Numerical Aperture
<i>NIR</i>	Near Infrared
<i>PCA</i>	Principal Component Analysis
<i>PLS</i>	Partial Least Squares
<i>RR</i>	Resonance Raman
<i>SERS</i>	Surface-Enhanced Raman Scattering
<i>SNR</i>	Signal-to-Noise Ratio
<i>UV</i>	Ultraviolet

References

- [1] Raman, Chandrasekhara Venkata, and Kariamanikkam Srinivasa Krishnan. "A new type of secondary radiation." *Nature* 121, no. 3048 (1928): 501-502.
- [2] Dorney, Timothy D., Richard G. Baraniuk, and Daniel M. Mittleman. "Material parameter estimation with terahertz time-domain spectroscopy." *JOSA A* 18, no. 7 (2001): 1562-1571.
- [3] Cloarec, Olivier, Marc-Emmanuel Dumas, Andrew Craig, Richard H. Barton, Johan Trygg, Jane Hudson, Christine Blancher et al. "Statistical total correlation spectroscopy: an exploratory approach for latent biomarker identification from metabolic ¹H NMR data sets." *Analytical Chemistry* 77, no. 5 (2005): 1282-1289.
- [4] Kmmmerle, Michael, Siegfried Scherer, and Herbert Seiler. "Rapid and reliable identification of food-borne yeasts by Fourier-transform infrared spectroscopy." *Applied and environmental microbiology* 64, no. 6 (1998): 2207-2214.
- [5] White, Sheri N. "Laser Raman spectroscopy as a technique for identification of seafloor hydrothermal and cold seep minerals." *Chemical Geology* 259, no. 3 (2009): 240-252.
- [6] Rai, Prakash, Srivalleesha Mallidi, Xiang Zheng, Ramtin Rahmanzadeh, Youssef Mir, Stefan Elrington, Ahmat Khurshid, and Tayyaba Hasan. "Development and applications of photo-triggered theranostic agents." *Advanced drug delivery reviews* 62, no. 11 (2010): 1094-1124. Hasan, Adv. Drug Del. Rev. 62 (2010) 1094-1124.
- [7] Rahmani, Zahra, Majid Kermani, Mitra Gholami, Ahmad Jonidi Jafari, and Niyaz Mohammad Mahmoodi. "Effectiveness of photochemical and sonochemical processes in degradation of Basic Violet 16 (BV16) dye from aqueous solutions." *Iranian journal of environmental health science and engineering* 9, no. 1 (2012): 1-7.

- [8] Wu, Ming-Chung, Min-Ping Lin, Shih-Wen Chen, Pei-Huan Lee, Jia-Han Li, and Wei-Fang Su. "Surface-enhanced Raman scattering substrate based on a Ag coated monolayer array of SiO₂ spheres for organic dye detection." *RSC Advances* 4, no. 20 (2014): 10043-10050.
- [9] Amer, M. S. *Raman Spectroscopy, Fullerenes and Nanotechnology*. Royal Society of Chemistry: Cambridge, United Kingdom, 2010; pp 43-44.
- [10] Ferraro, John R. *Introductory raman spectroscopy*. Academic press, 2003.
- [11] Lewis, Ian R., and Howell Edwards. *Handbook of Raman spectroscopy: from the research laboratory to the process line*. CRC Press, 2001.
- [12] Hanlon, E. B., R. Manoharan, T W Koo, K. E. Shafer, J. T. Motz, M. Fitzmaurice, J. R. Kramer, I. Itzkan, R. R. Dasari, and M. S. Feld. "Prospects for in vivo Raman spectroscopy." *Physics in medicine and biology* 45, no. 2 (2000): R1.
- [13] Choo-Smith, L.P., Edwards, H.G.M., Endtz, H.P., Kros, J.M., Heule, F., Barr, H., Robinson, J.S., Bruining, H.A., and Puppels, G.J. (2002) Medical applications of Raman spectroscopy: From proof of principle to clinical implementation. *Biopolymers*, 67 (1): 19.
- [14] Huang, Z.W., McWilliams, A., Lui, H., McLean, D.I., Lam, S., and Zeng, H.S. (2003) Nearinfrared Raman spectroscopy for optical diagnosis of lung cancer. *Int. J. Canc.*, 107 (6): 10471052.
- [15] Shafer-Peltier, K.E., Haka, A.S., Fitzmaurice, M., Crowe, J., Myles, J., Dasari, R.R., and Feld, M.S. (2002) Raman microspectroscopic model of human breast tissue: Implications for breast cancer diagnosis in vivo. *J. Raman Spectros.*, 33 (7): 552563.
- [16] Gazi, E., Dwyer, J., Gardner, P., Ghanbari-Siahkali, A., Wade, A.P., Miyan, J., Lockyer, N.P., Vickerman, J.C., Clarke, N.W., Shanks, J.H., Scott, L.J., Hart, C.A., and Brown, M. (2003) Applications of Fourier transform infrared microspectroscopy in studies of benign prostate and prostate cancer. A pilot study. *J. Pathol.*, 201 (1): 99108.
- [17] Hassing, S., K. D. Jernshj, and L. S. Christensen. *Raman Spectroscopy: A Non-Destructive and On-Site Tool for Control of Food Quality?*. INTECH Open Access Publisher, 2012.

- [18] Everall, Neil, Thomas Hahn, Pavel Matousek, Anthony W. Parker, and Michael Towrie. "Picosecond time-resolved Raman spectroscopy of solids: capabilities and limitations for fluorescence rejection and the influence of diffuse reflectance." *Applied spectroscopy* 55, no. 12 (2001): 1701-1708.
- [19] Song, Loling, E. J. Hennink, I. Ted Young, and Hans J. Tanke. "Photobleaching kinetics of fluorescein in quantitative fluorescence microscopy." *Biophysical journal* 68, no. 6 (1995): 2588.
- [20] Cadusch, P. J., M. M. Hlaing, S. A. Wade, S. L. McArthur, and P. R. Stoddart. "Improved methods for fluorescence background subtraction from Raman spectra." *Journal of Raman Spectroscopy* 44, no. 11 (2013): 1587-1595.
- [21] Pawley, James B. "Fundamental limits in confocal microscopy." In *Handbook of biological confocal microscopy*, pp. 20-42. Springer US, 2006.
- [22] Poborchii, Vladimir, Tetsuya Tada, and Toshihiko Kanayama. "Giant heating of Si nanoparticles by weak laser light: Optical microspectroscopic study and application to particle modification." *Journal of applied physics* 97, no. 10 (2005): 104323-104323.
- [23] Hibbert, R., and M. C. Price. "CHARACTERISATION OF RAMAN SPECTRA OF HIGH PURITY OLIVINE AS A FUNCTION OF TEMPERATURE AND SHOCK HISTORY: PREPARATION FOR EXOMARS." In *Lunar and Planetary Science Conference*, vol. 45, p. 1350. 2014.
- [24] Kouteva-Arguirova, Simona, Tz Arguirov, Dirk Wolfframm, and Jrgen Reif. "Influence of local heating on micro-Raman spectroscopy of silicon." *Journal of applied physics* 94, no. 8 (2003): 4946-4949.
- [25] Sato, H., Yamamoto, Y.S., Maruyama, A., Katagiri, T., Matsuura, Y., and Ozaki, Y. (2009) Raman study of brain functions in live mice and rats: A pilot study. *Vib. Spectros.*, 50 (1): 125130.
- [26] Kohler, M., Machill, S., Salzer, R., and Krafft, C. (2009) Characterization of lipid extracts from brain tissue and tumors using Raman spectroscopy and mass spectrometry. *Anal. Bioanal. Chem.*, 393 (5): 15131520.
- [27] Kirsch, M., Schackert, G., Salzer, R., and Krafft, C. (2010) Raman spectroscopic imaging for in vivo detection of cerebral brain metastases. *Anal. Bioanal. Chem.*, 398 (4): 17071713.

- [28] Vo-Dinh, Tuan. "Surface-enhanced Raman spectroscopy using metallic nanostructures." *TrAC Trends in Analytical Chemistry* 17, no. 8 (1998): 557-582.
- [29] Le Ru, Eric, and Pablo Etchegoin. *Principles of Surface-Enhanced Raman Spectroscopy: and related plasmonic effects*. Elsevier, 2008.
- [30] Lombardi, J.R.; Birke, R.L.; Lu, T.; Xu, J., Charge-transfer theory of surface enhanced Raman spectroscopy; Herzberg-Teller contributions; *J. Chem. Phys.* 1986, 84, 4174.
- [31] Sabur, Alia, Mickael Havel, and Yury Gogotsi. "SERS intensity optimization by controlling the size and shape of faceted gold nanoparticles." *Journal of Raman Spectroscopy* 39, no. 1 (2008): 61-67.
- [32] Yan, Bo, Anupama Thubagere, W. Ranjith Premasiri, Lawrence D. Ziegler, Luca Dal Negro, and Bjorn M. Reinhard. "Engineered SERS substrates with multiscale signal enhancement: nanoparticle cluster arrays." *Acs Nano* 3, no. 5 (2009): 1190-1202.
- [33] Boca, Sanda, Dumitrita Rugina, Adela Pintea, Lucian Barbu-Tudoran, and Simion Astilean. "Flower-shaped gold nanoparticles: synthesis, characterization and their application as SERS-active tags inside living cells." *Nanotechnology* 22, no. 5 (2011): 055702.
- [34] Boyack, Rufus, and Eric C. Le Ru. "Investigation of particle shape and size effects in SERS using T-matrix calculations." *Physical Chemistry Chemical Physics* 11, no. 34 (2009): 7398-7405.
- [35] Lee, Chang H., Limei Tian, Abdennour Abbas, Ramesh Kattumenu, and Srikanth Singamaneni. "Directed assembly of gold nanorods using aligned electrospun polymer nanofibers for highly efficient SERS substrates." *Nanotechnology* 22, no. 27 (2011): 275311.
- [36] Fan, Meikun, and Alexandre G. Brolo. "Silver nanoparticles self assembly as SERS substrates with near single molecule detection limit." *Physical Chemistry Chemical Physics* 11, no. 34 (2009): 7381-7389.
- [37] Huang, Shao Ying, Bae-Ian Wu, and Shaohui Foong. "Surface-enhanced Raman scattering enhancement factor distribution for nanoparticles of arbitrary shapes using surface integral equation method." *Journal of Applied Physics* 113, no. 4 (2013): 044304.
- [38] Lin, Hsing-Ying, Chen-Han Huang, Chih-Han Chang, Yun-Chiang Lan, and Hsiang-Chen Chui. "Direct near-field optical imaging of plasmonic resonances in metal nanoparticle pairs." *Optics express* 18, no. 1 (2010): 165-172.

- [39] Bergholt, Mads Sylvest, Shiyamala Duraipandian, Wei Zheng, and Zhiwei Huang. "Multivariate reference technique for quantitative analysis of fiber-optic tissue Raman spectroscopy." *Analytical chemistry* 85, no. 23 (2013): 11297-11303.
- [40] Cull, E. C., M. E. Gehm, B. D. Guenther, and D. J. Brady. "Standoff Raman spectroscopy system for remote chemical detection." In *Optics East 2005*, pp. 59940H-59940H. International Society for Optics and Photonics, 2005.
- [41] Mason, William T., ed. *Fluorescent and luminescent probes for biological activity: a practical guide to technology for quantitative real-time analysis*. Academic Press, 1999.
- [42] Strachan, Clare J., Thomas Rades, Keith C. Gordon, and Jukka Rantanen. "Raman spectroscopy for quantitative analysis of pharmaceutical solids." *Journal of pharmacy and pharmacology* 59, no. 2 (2007): 179-192.
- [43] Pelletier, M. J. "Quantitative analysis using Raman spectrometry." *Applied spectroscopy* 57, no. 1 (2003): 20A-42A.
- [44] Rantanen, Jukka, Hakan Wikstrm, Francis E. Rhea, and Lynne S. Taylor. "Improved understanding of factors contributing to quantification of anhydrate/hydrate powder mixtures." *Applied Spectroscopy* 59,no.7 (2005): 942951.
- [45] Currie, Lloyd A. "Nomenclature in evaluation of analytical methods including detection and quantification capabilities (IUPAC Recommendations 1995)." *Pure and Applied Chemistry* 67, no. 10 (1995): 1699-1723.
- [46] Munch, David J., Mike Wasko, Elizabeth Flynt, Steven C. Wendelken, Jenny Scifres, John R. Mario, Margo Hunt et al. "Validation and Peer Review of US Environmental Protection Agency Chemical Methods of Analysis." (2005).
- [47] Chang, K. H. "Limit of detection and its establishment in analytical chemistry." *Health Env J* 2 (2011): 38-43.
- [48] Armbruster, David A., and Terry Pry. "Limit of blank, limit of detection and limit of quantitation." *Clin Biochem Rev* 29, no. Suppl 1 (2008): S49-52.
- [49] Williams, K. P. J., G. D. Pitt, D. N. Batchelder, and B. J. Kip. "Confocal Raman microspectroscopy using a stigmatic spectrograph and CCD detector." *Applied spectroscopy* 48, no. 2 (1994): 232-235.

- [50] He, Xiaoxiao, Xu Wu, Kemin Wang, Bihua Shi, and Luo Hai. "Methylene blue-encapsulated phosphonate-terminated silica nanoparticles for simultaneous in vivo imaging and photodynamic therapy." *Biomaterials* 30, no. 29 (2009): 5601-5609.
- [51] Nuntawong, Noppadon, Mati Horprathum, Pitak Eiamchai, Krongkamol Wong-Ek, Viyapol Patthanasettakul, and Pongpan Chindaudom. "Surface-enhanced Raman scattering substrate of silver nanoparticles depositing on AAO template fabricated by magnetron sputtering." *Vacuum* 84, no. 12 (2010): 1415-1418.
- [52] Bergholt, Mads Sylvest, Shiyamala Duraipandian, Wei Zheng, and Zhiwei Huang. "Multivariate reference technique for quantitative analysis of fiber-optic tissue Raman spectroscopy." *Analytical chemistry* 85, no. 23 (2013): 11297-11303.
- [53] Cull, E. C., M. E. Gehm, B. D. Guenther, and D. J. Brady. "Standoff Raman spectroscopy system for remote chemical detection." In *Optics East 2005*, pp. 59940H-59940H. International Society for Optics and Photonics, 2005.
- [54] Wu, Ming, Mark Ray, K. Hang Fung, Mark W. Ruckman, David Harder, and Arthur J. Sedlacek. "Stand-off detection of chemicals by UV Raman spectroscopy." *Applied Spectroscopy* 54, no. 6 (2000): 800-806.
- [55] Dutta Roy, Sannak, Manash Ghosh, and Joydeep Chowdhury. "Adsorptive parameters and influence of hot geometries on the SER (R) S spectra of methylene blue molecules adsorbed on gold nanocolloidal particles." *Journal of Raman Spectroscopy* 46, no. 5 (2015): 451-461.
- [56] McCormack, Stephanie, and Donna L. Ross. "Teaching with technology." *The Science Teacher* 77, no. 7 (2010): 40.
- [57] Deegan, Robert D., Olgica Bakajin, Todd F. Dupont, Greb Huber, Sidney R. Nagel, and Thomas A. Witten. "Capillary flow as the cause of ring stains from dried liquid drops." *Nature* 389, no. 6653 (1997): 827-829.
- [58] Gupta, V. K. "Application of low-cost adsorbents for dye removal A review." *Journal of environmental management* 90, no. 8 (2009): 2313-2342.
- [59] Gerlach, Gerald, and Wolfram Dotzel. *Introduction to microsystem technology: a guide for students*. John Wiley and Sons, 2008.

- [60] Taylor, John R., and E. R. Cohen. "An introduction to error analysis: the study of uncertainties in physical measurements." *Measurement Science and Technology* 9, no. 6 (1998): 1015.
- [61] Hermosilla, I., G. Lopez-Reyes, A. Catala, A. Sanz, D. R. Llanos, and F. Rull. "Raman spectra processing algorithms and database for RLS-ExoMars." In *European Planetary Science Congress 2012*, vol. 1, p. 567. 2012.
- [62] Bocklitz, Thomas, Angela Walter, Katharina Hartmann, Petra Rsch, and Jrgen Popp. "How to pre-process Raman spectra for reliable and stable models?." *Analytica chimica acta* 704, no. 1 (2011): 47-56.
- [63] Dunn, Patrick F. *Measurement and data analysis for engineering and science*. CRC press, 2014.
- [64] Hanselman, Duane C., and Bruce Littlefield. *MATLAB; Version 4: User's Guide*. Prentice Hall PTR, 1995.
- [65] Shrivastava, Alankar, and Vipin B. Gupta. "Methods for the determination of limit of detection and limit of quantitation of the analytical methods." *Chronicles of Young Scientists* 2, no. 1 (2011): 21.
- [66] Matousek, Pavel, and Michael Morris, eds. *Emerging Raman applications and techniques in biomedical and pharmaceutical fields*. Springer Science and Business Media, 2010.
- [67] Macdonald, A. M., and P. Wyeth. "On the use of photobleaching to reduce fluorescence background in Raman spectroscopy to improve the reliability of pigment identification on painted textiles." *Journal of Raman Spectroscopy* 37, no. 8 (2006): 830-835.
- [68] Esposito, Anthony P., Chad E. Talley, Thomas Huser, Christopher W. Hollars, Charlene M. Schaldach, and Stephen M. Lane. "Analysis of single bacterial spores by micro-Raman spectroscopy." *Applied spectroscopy* 57, no. 7 (2003): 868-871.
- [69] Leach, R. K., ed. *Optical measurement of surface topography*. Vol. 81. Berlin: Springer, 2011.
- [70] Suetaka, W. *Surface infrared and Raman spectroscopy: methods and applications*. Vol. 3. Springer Science and Business Media, 2013.

- [71] Bugay, David E. "Characterization of the solid-state: spectroscopic techniques." *Advanced Drug Delivery Reviews* 48, no. 1 (2001): 43-65.
- [72] Roberts, Sarra N. Campbell, Adrian C. Williams, Ian M. Grimsey, and Steven W. Booth. "Quantitative analysis of mannitol polymorphs. FT-Raman spectroscopy." *Journal of pharmaceutical and biomedical analysis* 28, no. 6 (2002): 1135-1147.
- [73] Vergote, Geert J., Chris Vervaet, Jean Paul Remon, Tony Haemers, and Francis Verpoort. "Near-infrared FT-Raman spectroscopy as a rapid analytical tool for the determination of diltiazem hydrochloride in tablets." *European journal of pharmaceutical sciences* 16, no. 1 (2002): 63-67.
- [74] Everall, Neil J. "Confocal Raman microscopy: common errors and artefacts." *Analyst* 135, no. 10 (2010): 2512-2522.
- [75] Everall, Neil. "The influence of out-of-focus sample regions on the surface specificity of confocal Raman microscopy." *Applied spectroscopy* 62, no. 6 (2008): 591-598.
- [76] Macdonald, A. M., and A. S. Vaughan. "Numerical simulations of confocal Raman spectroscopic depth profiles of materials: a photon scattering approach." *Journal of Raman Spectroscopy* 38, no. 5 (2007): 584-592.
- [77] Brown, Matthew S., and Craig B. Arnold. "Fundamentals of laser-material interaction and application to multiscale surface modification." In *Laser precision microfabrication*, pp. 91-120. Springer Berlin Heidelberg, 2010.
- [78] Whang, Thou-Jen, Hsien-Yu Huang, Mu-Tao Hsieh, and Jyun-Jen Chen. "Laser-induced silver nanoparticles on titanium oxide for photocatalytic degradation of methylene blue." *International journal of molecular sciences* 10, no. 11 (2009): 4707-4718.
- [79] Habibalahi, A., and M. S. Safizadeh. "Pulsed eddy current and ultrasonic data fusion applied to stress measurement." *Measurement Science and Technology* 25, no. 5 (2014): 055601.
- [80] Gibbons, Robert D., and David E. Coleman. *Statistical methods for detection and quantification of environmental contamination*. John Wiley and Sons, 2001.